bioRxiv preprint doi: https://doi.org/10.1101/2024.10.10.617533; this version posted October 1, 2026. The copyright holder for this preprint (which was not certified by peer review) is the author/funder, who has granted bioRxiv a license to display the preprint in perpetuity. It is made available under a CC-BY 4.0 International license.

A single complex V2 as an alternative hypothesis for the organization of mouse higher visual cortex

Declan P. Rowley[1], Mary Beth Cassity[2]*, Jimin Park[3]*, Ryan Gillis[3]*, Julien Corbo[4], Casey Lennon-Jones[3], Severine Durand[3], R. Carter Peene[3], Avalon Amaya[3], Hannah Belski[3], Ivana Bussi[3], Tye Johnson[3], Jaimie Kenney[3], Henry Loeffler[3], Robyn Naidoo[3], Ben Ouellette[3], Alex Stearns[3], Jackie Swapp[3], Madeline Tom[3], Julie Weber[3], Josh Wilkes[3], Allison Williford[3], Shiella Caldejon[3], Peter A. Groblewski[3], Jérôme A. Lecoq[3], and Madineh Sedigh-Sarvestani[2,5]†

[1]Department of Ophthalmology and Fuster Laboratory for Cognitive Neuroscience, David Geffen School of Medicine, UCLA, Los Angeles, CA, USA
[2]Department of Neurobiology and Behavior, Cornell University, Ithaca, NY, USA
[3]Allen Institute, Neural Dynamics, Seattle, WA, USA
[4]Center for Molecular and Behavioral Neuroscience, Rutgers University–Newark, Newark, NJ, USA
[5]Howard Hughes Medical Institute, Cornell University, Ithaca, NY, USA

*These authors contributed equally to this work.
†Corresponding author: msarvestani@cornell.edu

Abstract:

The mouse has become a major model for studies of the visual system, creating a need for principles of areal delineation that can be compared across species. In many well-studied mammals, V1 is bordered by a single second visual area, V2, whereas the cortex immediately surrounding mouse V1 is commonly parcellated into roughly eight higher-order visual areas (HVAs), with boundaries defined in part by reversals in the progression of the visual field. However, work in other species has shown that such reversals can occur within a single visual area when retinotopic mapping is complex. This raises the possibility that some conventionally defined mouse HVAs may instead be subdivisions of a single complex V2. We use simulations to show that complex retinotopy within a single visual area can generate multiple apparent areal borders beyond mouse V1, and show that visual-field position contributes to reported functional differences among HVAs. We also release a large-scale Allen Institute OpenScope dataset comprising electrophysiological and two-photon recordings across V1**.** As an initial application of this resource, we examined response properties associated with visual cortical hierarchy and found that they clearly distinguished V1 from higher visual cortex, while variation among individual HVAs did not significantly exceed variation across sampled locations within V1. Together, these results motivate the unified-V2 hypothesis as an alternative model of mouse higher visual cortex while emphasizing that areal boundaries are most strongly supported when independent topographic, functional, architectonic, and connectional features exhibit reproducible, spatially coincident transitions. The OpenScope dataset provides a resource for independent tests of this and alternative models of mouse visual cortical organization.

bioRxiv preprint doi: https://doi.org/10.1101/2024.10.10.617533; this version posted October 1, 2026. The copyright holder for this preprint (which was not certified by peer review) is the author/funder, who has granted bioRxiv a license to display the preprint in perpetuity. It is made available under a CC-BY 4.0 International license.

Beyond V1, the mouse visual cortex has been parcellated into many higher order visual areas (Figure 1A). These modern area delineations draw on anatomical connectivity and functional retinotopic mapping (Garrett et al., 2014; Wang & Burkhalter, 2007; Zhuang et al., 2017), with reversals in the progression of the visual field serving as an important criterion for identifying areal boundaries (Figure 1A). Such reversals, also known as mirror maps, indicate a new map of the visual field, and therefore a new visual area, under the assumption of simple retinotopic mapping. However, recent work (Sedigh-Sarvestani et al., 2021; Sedigh-Sarvestani & Fitzpatrick, 2022; Yu et al., 2020) has shown that visual field reversals are a hallmark of complex retinotopic mapping within V2 and other higher order visual areas of primates and several other species (Figure 1B). This prompted us to ask whether some of the higher order areas of the mouse, delineated by reversals, may in fact be subdivisions of a single area V2 (Figure 1C). This could help explain the systematic and spatially organized biases in visual-field representation reported across higher visual cortex (Figure 1A, Zhuang et al., 2017). Nearby brain regions exhibit biased representation for nearby regions of the visual field, an organization consistent with a single area V2 exhibiting a complex map of the visual field.

The parcellation of higher order visual cortex in the mouse has evolved in recent decades (Glickfeld & Olsen, 2017) with different studies parcellating the cortex beyond V1 into between 2 and 16 areas (Zhuang et al., 2017). Projection and functional mapping studies provided increasingly detailed evidence for multiple retinotopic subdivisions beyond V1, establishing the parcellation that now dominates the field (Garrett et al., 2014; Wang & Burkhalter, 2007; Zhuang et al., 2017). However, this interpretation assumes that reversals and redundant representations mark boundaries between maps rather than structure within a complex map. Comparative work has long raised alternatives, including the proposal that repeated extrastriate modules may form subdivisions of a single V2 (Kaas et al., 1989; Malach, 1989; Rosa & Krubitzer, 1999).

In the past decade, we have gained a better understanding of the diversity of retinotopic transformations in visual areas. Specifically, we have gained structural and functional evidence that visual field reversals can occur in single visual areas when the retinotopic transform within that area is complex (Figure 1B). These reversals, and the underlying complex retinotopy, can be explained by wiring minimization principles related to visual field coverage constrained by the anatomy of cortex beyond V1, and have now been reported in tree shrews (Sedigh-Sarvestani et al., 2021), marmosets (Yu et al., 2020), ferrets (Manger et al., 2002) and squirrels (Kaas et al., 1989). Therefore, it is possible that mouse visual cortex also exhibits complex retinotopic mapping beyond V1, such that some reversals currently interpreted as areal boundaries could instead occur within a larger secondary visual area (Figure 1C). A unified V2 would also bring the criteria used to classify mouse higher visual cortex into closer alignment with those applied to complex secondary visual areas in other mammals (Figure 1D). More broadly, the discrepancy across species motivates asking whether a common set of criteria for areal delineation can be applied despite species-specific differences in cortical geometry and retinotopic organization.

Such an alternative organization of the mouse visual cortex intersects with a broader and longstanding question: what constitutes a cortical area? This is not merely a question of nomenclature: areal parcellations guide hypothesis formation, experimental targeting, and interpretation of regional differences in computation. The criteria used to define those boundaries therefore directly shape how cortical organization is studied and understood. Garrett et al. (2014) formalized four retinotopic criteria for identifying mouse visual areas: uniform visual field sign within an area, absence of redundant representation within an area, redundant representation between neighboring same-sign areas, and reproducibility of area location across experiments. Complex retinotopic maps in other species suggest that the first three criteria may need to be interpreted in the context of map geometry. In a simple monotonic map, a repeated representation encountered after progression through visual space provides strong evidence for a second map. In a complex map, however, local redundancy can arise within a single continuous area when the retinotopic transformation folds or reverses direction, causing neighboring portions of cortex to represent overlapping regions of visual space. Redundant representation therefore does not, by itself, distinguish a boundary between two maps from an internal fold within one complex

bioRxiv preprint doi: https://doi.org/10.1101/2024.10.10.617533; this version posted October 1, 2026. The copyright holder for this preprint (which was not certified by peer review) is the author/funder, who has granted bioRxiv a license to display the preprint in perpetuity. It is made available under a CC-BY 4.0 International license.

map. More generally, we consider topography to be one of several sources of evidence for areal boundaries, alongside functional specialization, architectonics, and connectivity. We therefore consider evidence for a distinct area strongest when multiple independent properties exhibit reproducible and spatially coincident transitions. Because functional, architectonic, and connectional properties can themselves covary with retinotopy, however, apparent convergence across modalities should only be treated as independent evidence when it cannot be explained by a shared topographic organization.

However, if many conventionally defined HVAs are subdivisions of a larger V2, how can we explain the functional differences reported among them? Reported differences among HVAs include spectral sensitivity, spatial and temporal frequency preference, receptive-field size, response latency, binocular disparity, and other response properties (Glickfeld et al., 2013; Marshel et al., 2011; Rhim et al., 2017; Sit & Goard, 2020). One possibility is that some of these functional differences reflect the different visual field biases of each region rather than areal identity per se (Sedigh-Sarvestani & Fitzpatrick, 2022). Importantly, these relationships need not take the form of a single monotonic gradient: functional properties may vary nonlinearly across visual space or along multiple retinotopic axes within a single visual area.

Here we use computational modeling, published anatomical and functional evidence, and reanalysis of existing datasets to test the hypothesis that many conventionally defined HVAs may instead constitute spatially organized, functionally distinct subdivisions of a single complex V2. We ask whether a single retinotopic map constrained by mouse cortical geometry can generate the reversals and projection patterns used to delineate HVAs, and to what extent functional differences among these regions may reflect their biased sampling of visual space rather than discrete areal identity. In addition, we release a new large-scale Allen Institute OpenScope dataset comprising electrophysiological and two-photon measurements across V1, including receptive-field mapping and characterization of orientation, spatial-frequency, and temporal-frequency tuning. As an initial application of this community resource, we ask how the magnitude of functional variation within V1 compares with differences used to characterize hierarchy among HVAs. By releasing the complete dataset, we also enable independent tests of the unified-V2 hypothesis by providing a within-area benchmark for evaluating the magnitude of functional differences among conventionally defined HVAs.

bioRxiv preprint doi: https://doi.org/10.1101/2024.10.10.617533; this version posted October 1, 2026. The copyright holder for this preprint (which was not certified by peer review) is the author/funder, who has granted bioRxiv a license to display the preprint in perpetuity. It is made available under a CC-BY 4.0 International license.

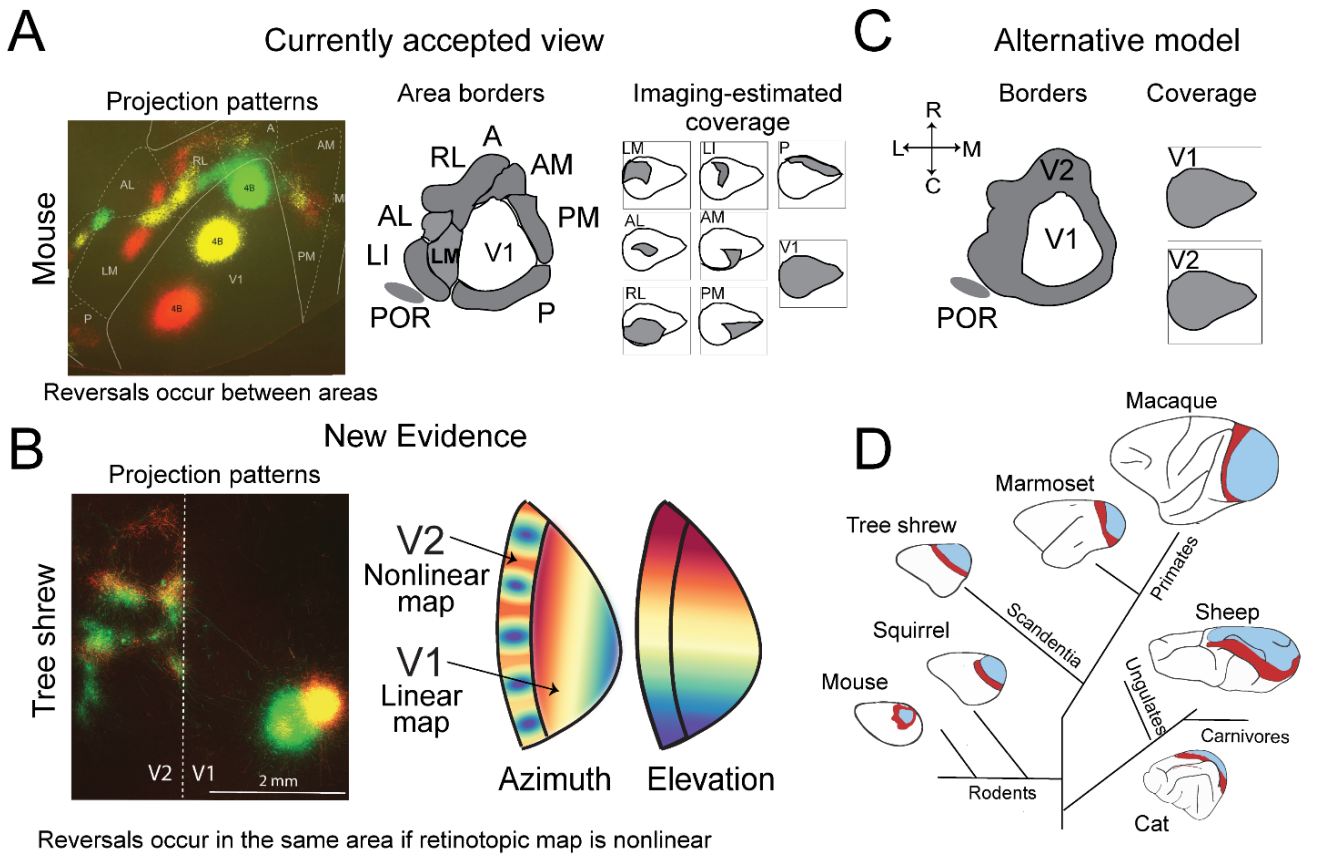

Figure 1: A single complex V2 as an alternative organization of mouse higher visual cortex. A) The currently accepted organization of the mouse visual system includes multiple higher order visual areas beyond V1, delineated using functional retinotopy together with anatomical connectivity. Individual HVAs exhibit overlapping but systematically biased representations of visual space. Projection pattern figure is modified from (Wang & Burkhalter, 2007) and visual field coverage maps are modified from (Zhuang et al., 2017). These imaging-based maps may underestimate absolute visual-field extent, but they reveal systematic differences in the distribution and weighting of visual space across HVAs. **B)** New evidence of visual field reversals within single areas in the tree shrew (Sedigh-Sarvestani et al., 2021) demonstrates that reversals do not necessarily indicate areal boundaries. **C)** We consider an alternative organization wherein many of the conventionally defined HVAs are subdivisions of a single area V2 in the mouse. **D)** Such an organization would bring the criteria used to delineate HVAs into closer alignment with those applied in several other species. Modified from (Rosa & Krubitzer, 1999).

Complex retinotopy within a single visual area can generate the appearance of multiple higher order areas in mouse visual cortex

The cortex immediately adjacent to mouse V1 was originally designated cytoarchitectonically as areas 18a (lateral) and 18b (medial) and early electrophysiological mapping identified a single area V2 within lateral 18a, bordered by V3, together with two smaller maps in medial 18b, as reviewed in (Glickfeld & Olsen, 2017). Subsequently, precisely localized multi-color projection studies (Wang & Burkhalter, 2007) revealed multiple topographically organized projection zones beyond V1. Subsequent functional retinotopic mapping identified multiple field-sign reversals and redundant representations, providing the basis for the HVA parcellation widely used today (Garrett et al., 2014; Zhuang et al., 2017). However, as discussed above, multiple visual field reversals can be a hallmark of complex retinotopic mapping within a single area (Sedigh-Sarvestani et al., 2021; Yu et al., 2020). We set out to explain the reversals beyond mouse V1 with an elastic net model of retinotopy, well-established for exploration of map organization in other species (Goodhill & Willshaw, 1990; Sedigh-

bioRxiv preprint doi: https://doi.org/10.1101/2024.10.10.617533; this version posted October 1, 2026. The copyright holder for this preprint (which was not certified by peer review) is the author/funder, who has granted bioRxiv a license to display the preprint in perpetuity. It is made available under a CC-BY 4.0 International license.

Sarvestani et al., 2021; Wolf et al., 1994; Yu et al., 2020). Here, we model the cortical region surrounding V1 as a single continuous area. Its cortical extent is constrained by the V1 border and a population-derived estimate of the surrounding extrastriate cortical footprint from Waters et al. (2019), rather than by the boundaries of individual HVAs. This simulated V2 consists of point "neurons," each with a receptive field (RF) in the visual field. The objective of the algorithm is to arrange the RFs so they uniformly tile the visual field with the wiring-length constraint of preserving map "smoothness"; e.g., nearby neurons on the cortex should have nearby RFs in the visual field. The algorithm iteratively optimizes the RFs to reduce the total cost associated with visual field coverage and smoothness until a stable state is reached.

To apply the modeling techniques used in previous papers, we first needed to account for key differences in anatomy of the mouse visual cortex, including the shape of the cortical sheet surrounding V1 and the extent and geometry of the mouse visual field represented in V1 (Figure 2A). Because the visual-field extent sampled by widefield imaging is restricted, particularly in elevation, we modeled a broader visual-field envelope spanning approximately 0–140° azimuth and −40–60° elevation, constrained by electrophysiological measurements from Wagor et al. (1980) and the rounded visual field coverage reported by Garrett et al. (2014). We modified the algorithm to weight the interactions between neighbors by the inverse square of their distance in cortical space to account for unevenly spaced nodes. In addition, we also expected a lower cost associated with the smoothness constraint due to larger receptive fields in the mouse visual system. The mouse's smaller eyes result in low spatial resolution as the visual field is projected through the pupil onto a smaller retinal surface. In V1 this results in much larger receptive fields and beyond this, allows for bigger steps in the visual field to be taken by adjacent regions of cortex while preserving an overlapping representation. Given this, we expected that a lower weight on the smoothness constraint in our model may result in a better representation of the higher order visual areas' retinotopy (Figure 2B-C).

Figure 2 shows the outcome of an example instance of the model simulating the mouse visual system beyond V1 using 640 neurons. A single elastic net model, constrained by the geometry of the cortical sheet surrounding V1 and trained to cover the mouse visual field, can generate retinotopy with reversals similar in number and scale to those reported in the mouse. Critically, these reversals are not imposed on the model; they emerge from the competing constraints of visual-field coverage, local map smoothness, and cortical geometry. As in previous work, modifying the weights associated with smoothness results in internal reversals, seen in alternating field sign (Sereno et al., 1994) (Figure 2C-E). The precise locations of these reversals vary with model parameters and initial conditions and are not intended as a fit to the empirical HVA map. Rather, the simulation provides proof of principle that an explicitly defined single visual area can develop a complex retinotopic map containing multiple field-sign reversals when constrained by the geometry of mouse cortex. We note that variation also exists in the reported retinotopy of the mouse between animals (Waters et al., 2019). Thus, the model demonstrates the feasibility of multiple reversals arising as structure within a single complex map, without imposing internal areal boundaries.

bioRxiv preprint doi: https://doi.org/10.1101/2024.10.10.617533; this version posted October 1, 2026. The copyright holder for this preprint (which was not certified by peer review) is the author/funder, who has granted bioRxiv a license to display the preprint in perpetuity. It is made available under a CC-BY 4.0 International license.

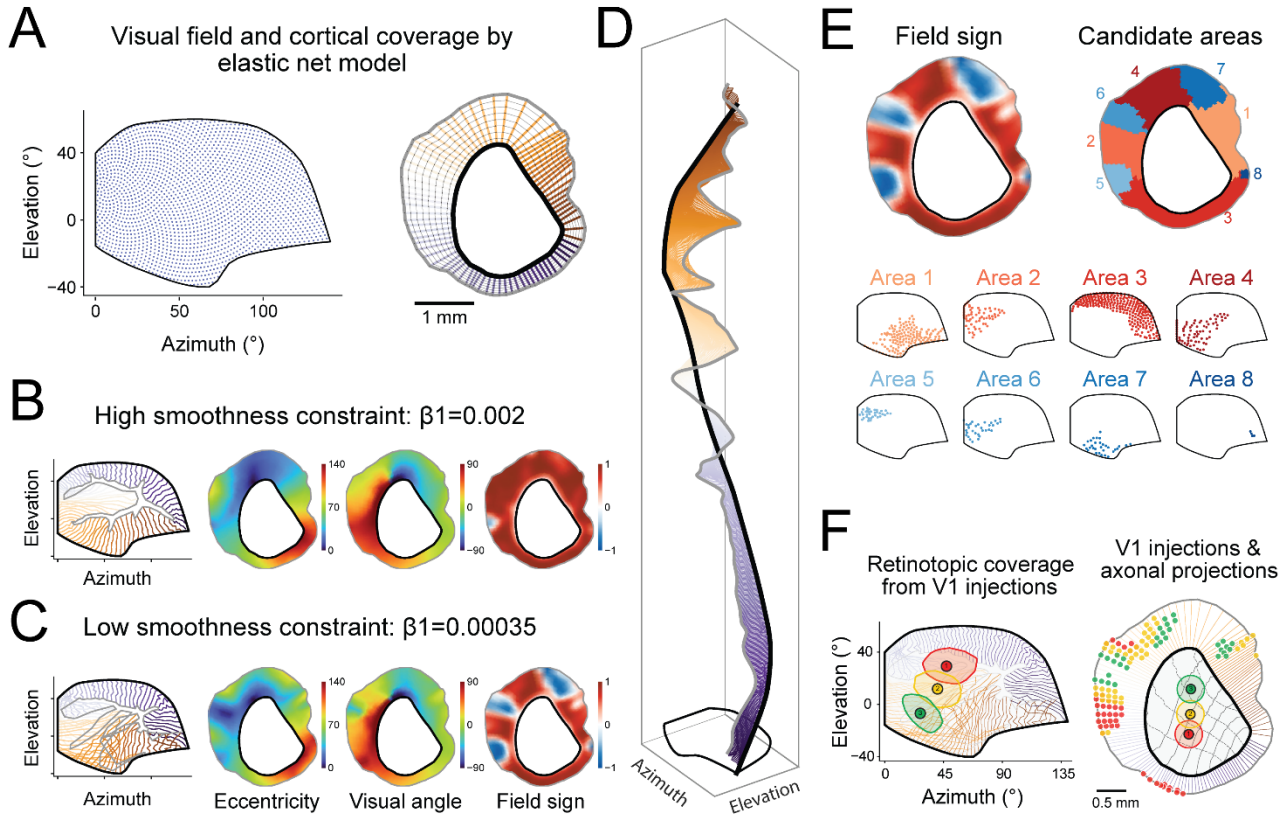

Figure 2: Retinotopic models show emergence of a single complex map of visual space beyond mouse V1. We extended the elastic net model from previous work (Sedigh-Sarvestani et al., 2021) to constrain a model of V2 to the unique structure of the mouse. **A)** The modeled cortical sheet is bounded internally by the V1 border and externally by a cortical footprint derived from Waters et al. (2019). The modeled visual-field domain was represented by a smooth envelope constrained by electrophysiological estimates of V1 coverage from Wagor et al. (1980; approximately 0–140° azimuth and −40–60° elevation) and the rounded coverage reported by Garrett et al. (2014). **B-C)** Modifying the smoothness constraint results in internal reversals, seen in alternating field sign (Sereno et al., 1994). **D)** The same model visualized as a series of cortical transects normal to the V1 border and extending to the outer boundary of higher visual cortex. Each transect is plotted in azimuth-elevation space and stacked around the V1 circumference (purple to orange). A simple monotonic map would form a smooth, untwisted sheet; the folds here reflect reversals in visual-field progression within the single modeled area. **E)** A single continuous model can generate multiple internal field-sign reversals (left). When the area-delineation rules of Garrett et al. (2014) are applied to this single map, nine candidate 'areas' result (right), each with a distinct bias in visual-field coverage. **F)** Simulated projections from 3 spatially segregated patches within V1 (Left), along with the resulting projection pattern of axons beyond V1 (right), illustrating how patchy projection patterns in retinotopically matched regions of visual space of V1 and a single higher order area can emerge from a complex retinotopic transform.

The complex nature of the single visual field covering higher order visual cortex is visualized in Figure 2D, where azimuth and elevation axes are plotted against each other in X and Y coordinates at the base, and the progression along the visual field as one moves on the cortical sheet around V1 is plotted on the Z-axis. In this visualization, a simple monotonic map would form a smooth, untwisted sheet. Thus, the folds in Figure 2D reflect reversals in visual-field progression within the single modeled area. These multiple internal reversals within a single continuous map are also shown in Figure 2E. Importantly, these reversals are accompanied by local redundancy in visual-field representation, even though the modeled cortical sheet is explicitly defined as a single continuous area. This redundancy arises from folds in the retinotopic transformation: as the map reverses direction, nearby cortical regions can sample overlapping portions of visual space. Thus, the model provides a

bioRxiv preprint doi: https://doi.org/10.1101/2024.10.10.617533; this version posted October 1, 2026. The copyright holder for this preprint (which was not certified by peer review) is the author/funder, who has granted bioRxiv a license to display the preprint in perpetuity. It is made available under a CC-BY 4.0 International license.

concrete example in which the combination of a field-sign reversal and redundant representation—features conventionally used to separate mouse HVAs—can emerge within a single map.

The apparent areas generated by the model differ systematically in their representation of visual space (Figure 2E). Although these regions arise only from partitioning a single continuous map, each exhibits a distinct bias toward particular portions of the visual field. Importantly, these biases are not independent: their preferred regions of visual space vary systematically with position around V1, such that neighboring cortical regions tend to represent neighboring portions of the visual field. This organization resembles the orderly differences in visual-field representation reported across mouse HVAs (Wang & Burkhalter, 2007; Garrett et al., 2014; Zhuang et al., 2017). Critically, this observation does not depend on whether individual HVAs contain complete or incomplete representations of the visual field. Even complete representations can be strongly biased toward particular locations. Rather, it is the systematic relationship between visual-field bias and cortical position across regions that is consistent with their being subdivisions of a larger continuous retinotopic map.

Because nearby locations in V1 project to retinotopically corresponding locations in higher visual cortex, we can also use the model to simulate the qualitative consequences of multi-color tracer injections into V1 (Figure 2F). The resulting projection patterns form multiple spatially segregated patches despite arising from a single modeled area. We do not expect this simple model to quantitatively reproduce the projection patterns reported by Wang & Burkhalter (2007); rather, the simulation demonstrates that segregated projection zones can arise from a single complex retinotopic transform and therefore do not, on their own, require multiple areal maps. Together, these simulations establish that the retinotopic reversals, the associated local redundancy in visual field representation, and segregated projection zones are geometrically compatible with a single complex visual area. The model does not establish that mouse higher visual cortex is a unified V2; instead, it demonstrates that these features are not uniquely diagnostic of multiple areas.

Functional organization across higher visual cortex is strongly structured by retinotopy

Functional feature differences are one of the main metrics used to justify areal definitions in the higher order visual system of primates and cats. For instance, area MT in primates exhibits sensitivity to global motion direction that is absent in area V2, even in identical regions of the visual field. Such hierarchical and parallel processing of overlapping parts of the visual field is thought to represent an efficient strategy to build selectivity to complex input features (Felleman & Van Essen, 1991).

Under the unified-V2 hypothesis, conventionally defined HVAs are considered functional modules of a single area, each with response properties related to its distinct visual field bias. It is important to be explicit about what this hypothesis does and does not require. It requires that functional differences among modules be organized by retinotopy, rather than forming discontinuities at conventional areal boundaries that are independent of visual-field position. It does not require that these retinotopically anchored differences be inherited from any particular input. We consider at least three, non-mutually exclusive, sources. First, the differences may already be present across the retinotopic map of V1 and simply conveyed to retinotopically matched locations in V2. Second, they may be delivered by subcortical pathways from the superior colliculus and the lateral posterior nucleus (LP). These regions project to higher visual cortex with strong retinotopic biases and functional response properties that differ across those biases (Tohmi et al., 2014; Bennett et al., 2019; Juavinett et al., 2020; Calzoni et al., 2026). Third, they may be generated within V2 itself, through target-specific selection of V1 inputs (Glickfeld et al., 2013) or through local circuitry. A retinotopically organized difference among modules is compatible with a single area under any of these sources, just as the stripes of macaque V2 differ in function and connectivity while remaining subdivisions of one area (Hubel & Livingstone, 1987; Livingstone & Hubel, 1984). What the hypothesis does require is that functional differences among modules be organized by retinotopy, varying smoothly with visual-field position and continuing across conventional areal boundaries, rather than forming discontinuities at those

bioRxiv preprint doi: https://doi.org/10.1101/2024.10.10.617533; this version posted October 1, 2026. The copyright holder for this preprint (which was not certified by peer review) is the author/funder, who has granted bioRxiv a license to display the preprint in perpetuity. It is made available under a CC-BY 4.0 International license.

boundaries that are independent of visual-field position. We first ask whether existing observations are consistent with this requirement, and then test it directly by reanalyzing a published dataset.

In the mouse higher order cortex, many reported functional properties vary continuously across multiple conventionally defined areas, rather than forming robust and sharp differences between areas as observed in primates (Figure 3). For instance, binocular disparity tuning (La Chioma et al., 2019), color tuning (Aihara et al., 2017), and coherent motion processing (Sit & Goard, 2020) have all been shown to vary across the elevation axis of retinotopy (Figure 3A). Cortical inputs to upper- and lower-visual field domains of the superior colliculus are strongly organized by visual field position across extrastriate cortex (Calzoni et al., 2026). These trends are consistent with the ethological relevance of visual field locations for a low-lying animal like the mouse (Qiu et al., 2021). Furthermore, the areas categorized into the dorsal and ventral streams of the mouse cortex also exhibit robust biases for the lower and upper visual field (Figure 3B). Functional property differences in higher order visual areas have also been reported to vary along the azimuth axis of retinotopy. Encoding of various behavioral task-related features was shown to vary across higher order visual areas of the mouse (Minderer et al., 2019), but as the authors point out, this variation is agnostic to higher order areal boundaries and instead follows the underlying topography smoothly (Figure 3C). In fact, the only functional discontinuities in the mouse posterior cortex were found at the major anatomical borders between V1, parietal, and retrosplenial areas. Finally, learning-related plasticity in the mouse visual system has been reported across broad medial and anterior higher-visual-cortex domains rather than individual named areas (Zhong et al., 2025). Together, these findings suggest that functional organization in higher visual cortex largely follows retinotopic or mesoscale cortical axes that traverse conventional HVA boundaries, rather than necessarily being organized into discrete area-specific domains.

If functional differences among HVAs partly reflect which portions of visual space they disproportionately sample, it is important to distinguish visual-field extent from visual-field bias. Electrophysiological recordings (Wagor et al., 1980; Wang et al., 2011; Wang & Burkhalter, 2007) indicate that some HVAs span broader regions of visual space than suggested by widefield imaging, whereas functional imaging reveals substantial overlap together with strong differences in the relative weighting of visual-field locations (Garrett et al., 2014; Zhuang et al., 2017). Importantly, these biases are spatially organized, such that neighboring HVAs preferentially represent neighboring portions of visual space (Figure 1A). Thus, our argument does not require incomplete visual-field coverage: even if individual HVAs ultimately prove to span the full visual field, their systematically different weighting of central, peripheral, upper, and lower visual space could produce substantial differences in population-averaged response properties. Uncertainty in absolute extent therefore does not remove the orderly retinotopic biases most relevant to our functional argument.

Such observations raise the possibility that some functional differences among mouse HVAs reflect their systematically different weighting of the retinotopic map rather than discrete areal identity (Groen et al., 2022; Kanwisher, 2001; Sedigh-Sarvestani & Fitzpatrick, 2022; Yu & Rosa, 2014). Testing this hypothesis requires careful measurements of visual field location and functional property differences in V1 and higher order visual areas. Such data sets are sparse but growing. To test our hypothesis with existing data, we reanalyzed a dataset from Han et al. (2022) and found that accounting for eccentricity and elevation reduced some of the reported differences in spatial- and temporal-frequency tuning among HVAs (Figure 3). The relationship of tuning with eccentricity is unexpectedly inverted relative to the classic trend reported in primate visual cortex, but is nonetheless still smooth.

In primate vision research ‘eccentricity’ is used to mean distance in visual degrees from the center of gaze, which is a useful metric for animals with a fovea and robust overrepresentation of the central few degrees of vision. Many functional properties scale with eccentricity within visual areas, making it a very important parameter to control for in foveal animals such as primates (Yu et al., 2015). However, in the afoveate mouse, ‘center of gaze’ is difficult to control for and typically elevation above eye level and azimuth relative to a normal through the eye

bioRxiv preprint doi: https://doi.org/10.1101/2024.10.10.617533; this version posted October 1, 2026. The copyright holder for this preprint (which was not certified by peer review) is the author/funder, who has granted bioRxiv a license to display the preprint in perpetuity. It is made available under a CC-BY 4.0 International license.

are used. While this is a reasonable approach for an animal without a fovea, a central region of the upper binocular visual field of the mouse, named the 'focea', has been reported to have enhanced spatial resolution: V1 population receptive fields are smallest there, single-neuron receptive fields in LM and AL are smallest there, and behavioral acuity is highest there (van Beest et al., 2021). Notably, this region is not associated with increased cortical magnification in V1; the enhanced resolution reflects reduced receptive-field scatter and overrepresentation of binocular space rather than a foveal-like expansion of the map (van Beest et al., 2021). The focea nonetheless provides a natural reference point for a mouse analog of eccentricity. Taking the focea as 20 degrees above resting eye level on the vertical meridian (0 degrees azimuth), we defined 'eccentricity' (Figure 3D) as the Euclidean distance from this point in degrees of visual field, and assessed functional properties as a function of this distance.

There is an additional effect across retinotopy in the mouse that must be considered. The mouse retina has a gradient of cone opsin expression (Figure 3E) such that S-opsin, sensitive to UV light, is overrepresented on the ventral surface (the upper visual field) and gives way to M-opsin, sensitive to green light, on the dorsal surface (the lower visual field). When a typical LCD monitor is used, relatively more M-cones, compared to S-cones, are partially activated (Rhim et al., 2021). This means that retinal regions in the upper and lower visual fields are in a rod-dominated scotopic and mixed cone- and rod- mediated mesopic regime respectively. This retinal gradient is known to be preserved in the visual cortex (Rhim et al., 2017) and is thought to play an important role in predator evasion (Qiu et al., 2021). Thus, control for the opsin gradient is crucial for accurate measurement, reporting, and comparative analysis of functional properties in mice. Specifically, the use of typical LCD monitors results in primacy of scotopic vision in the ventral retina, producing higher spatial and lower temporal frequency tuning in the upper visual field.

In Han et al. (2022), an LCD screen was used. The observed trend, albeit small, toward higher SF tuning in areas with predominantly upper-field representations (Figure 3F) suggests that the cone-opsin gradient may contribute. To estimate the contribution of retinotopic position, we registered individual cells to the Zhuang et al. (2017) azimuth and elevation maps and fit SF and TF preference as a function of elevation and eccentricity from the focea (Figure 3F–G; Methods). Subtracting the fitted retinotopic component reduced some of the differences in mean SF and TF tuning among higher order areas. This suggests that visual-field position contributes to measured functional differences among HVAs. We emphasize that this analysis is agnostic to the source of the retinotopic component it removes: the fitted plane describes how tuning varies with retinotopy across higher visual cortex, regardless of whether that variation is inherited from V1, from subcortical regions, or generated within V2. It also leaves open residual differences not captured by retinotopy, or those with more complex nonmonotonic relationships with retinotopy.

bioRxiv preprint doi: https://doi.org/10.1101/2024.10.10.617533; this version posted October 1, 2026. The copyright holder for this preprint (which was not certified by peer review) is the author/funder, who has granted bioRxiv a license to display the preprint in perpetuity. It is made available under a CC-BY 4.0 International license.

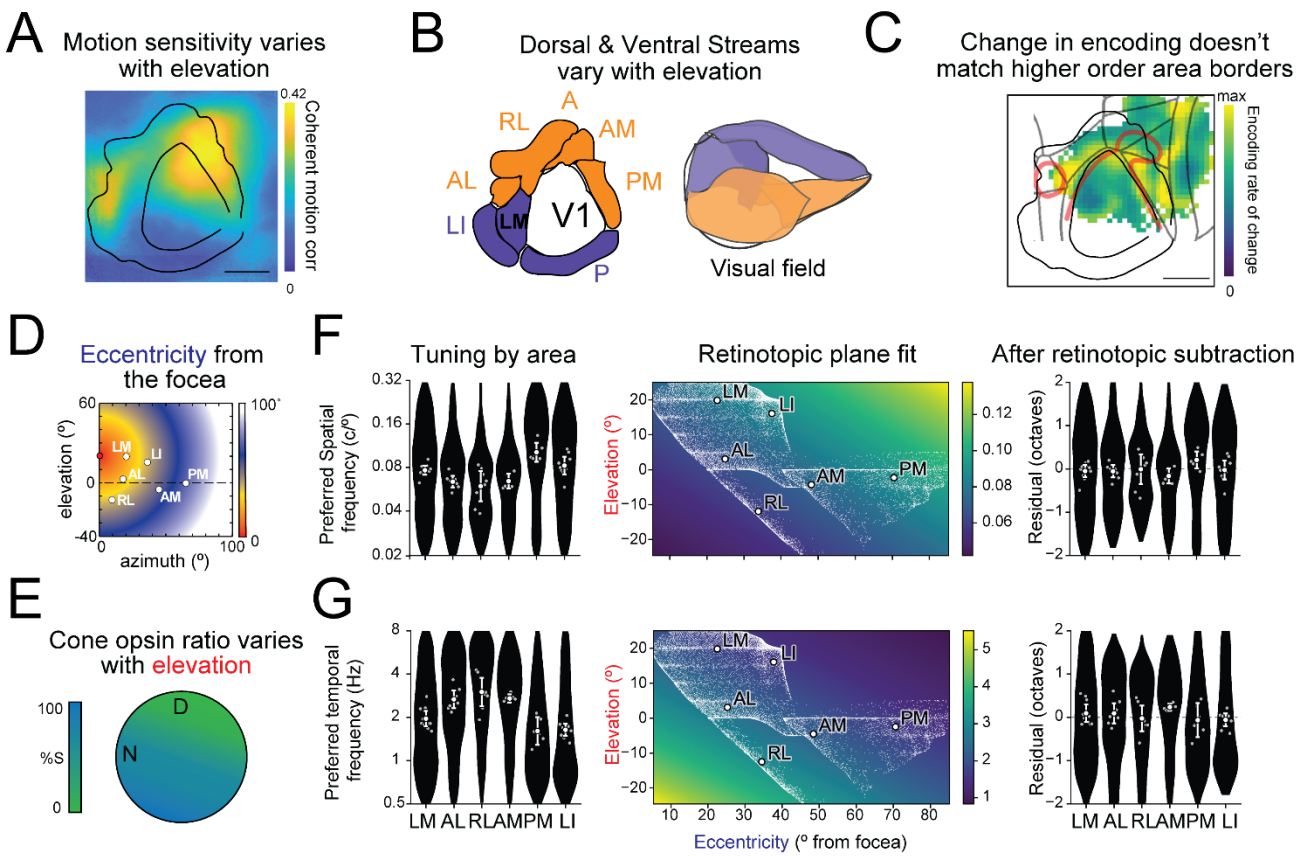

Figure 3: Retinotopic position contributes to functional variation across mouse higher visual cortex. A) Map of motion sensitivity adapted from (Sit & Goard, 2020) showing higher sensitivity in the lower field representation of V1 and higher order visual areas. **B)** Dorsal and Ventral streams in the mouse containing multiple higher order visual areas have been suggested due to differences in function, however these maps closely align onto elevation axis of retinotopy. Figure made using data from Zhuang et al. (2017) **C)** Behavioral encoding as a function of cortical space shows large change along the V1 border, but not between higher order visual areas (Minderer et al., 2019). Scale bar 1mm. **D)** Schematic of eccentricity from focea with area estimates for the data used in F&G. **E)** Schematic of retinal cone opsin gradient following (Demb & Singer, 2015). **F–G)** Reanalysis of Han et al. (2022) examining spatial- and temporal-frequency tuning before and after accounting for estimated retinotopic position. F) Preferred spatial frequency (SF). Left, cell-level tuning distributions across six higher visual areas. Middle, fitted SF as a function of elevation and eccentricity from the focea. Small white points indicate estimated retinotopic positions of individual cells included in the fit; large white points indicate the mean retinotopic position of the cells displayed for each area. Color indicates fitted SF. Right, residuals after subtracting the fitted retinotopic component; the dashed line indicates zero. Gray points show individual-mouse means, and large white points and bars show the equally weighted mean across mice and its 95% confidence interval. G) Same as F for preferred temporal frequency (TF). Plane fits included censored values at the analysis bounds; distributions and residual summaries include cells within those bounds (see Methods).

We note that changes in spatial and temporal frequency, varying smoothly with eccentricity, have been observed in visual areas of various species including primates (Sedigh-Sarvestani & Fitzpatrick, 2022; Yu et al., 2010). However, in the case of spatial frequency, the relationship we observe across mouse higher visual cortex appears to be inverted from that observed in primate V1 (Yu et al., 2010). In our reanalysis of Han et al. (2022), preference for higher spatial frequencies increases with eccentricity from the focea rather than decreasing (Figure 3F). We are not aware of a prior report of this relationship in mouse higher visual cortex; Han et al. (2022) and Marshel et al. (2011) reported area-level SF differences without analyzing SF as a function of retinotopic position, and Marshel et al. (2011) restricted their comparisons to eccentricity-matched neurons near the central visual field. Such an inverse relationship between SF preference and eccentricity does not impact our argument that functional feature differences vary smoothly across multiple areas, rather than sharply between them. It does bear

bioRxiv preprint doi: https://doi.org/10.1101/2024.10.10.617533; this version posted October 1, 2026. The copyright holder for this preprint (which was not certified by peer review) is the author/funder, who has granted bioRxiv a license to display the preprint in perpetuity. It is made available under a CC-BY 4.0 International license.

on the source of these differences. The few available measurements within V1 show smaller receptive fields and higher behavioral acuity for the focea, the central region of the upper visual field, and a cutoff SF that increases with elevation (Zhang et al., 2015; van Beest et al., 2021). Taken at face value, this would suggest that the SF gradient across V2 modules is not simply inherited from V1. However, the evidence is sparse, the V1 and HVA measurements come from different stimuli and methods, and the cone-opsin gradient confounds both under conventional display conditions. Resolving this requires functional properties measured as a function of receptive-field position across V1 and across higher visual cortex under matched conditions; the OpenScope dataset released here provides the V1 half of that comparison.

Large-scale OpenScope recordings provide a within-area benchmark for functional heterogeneity

To more directly assess how much functional variation can occur within a single cortical area, we collected a new large-scale dataset through the Allen Institute OpenScope program. The dataset includes electrophysiological recordings from four targeted V1 locations per mouse as well as two-photon imaging recordings from 12 targeted V1 locations per mouse (Figure 4A-B). Electrophysiological data were collected for eight mice, each with four probes targeting different regions of V1 (Figure 4A). Two-photon recordings from 12 fields of view (Figure 4B), each sampled at two depths, were recorded in six mice. Visual stimuli were designed to map receptive-field location and characterize orientation, spatial-frequency, and temporal-frequency tuning. The complete dataset and preliminary analysis code are released with this study to enable independent analyses of functional organization across V1 and tests of the unified-V2 hypothesis.

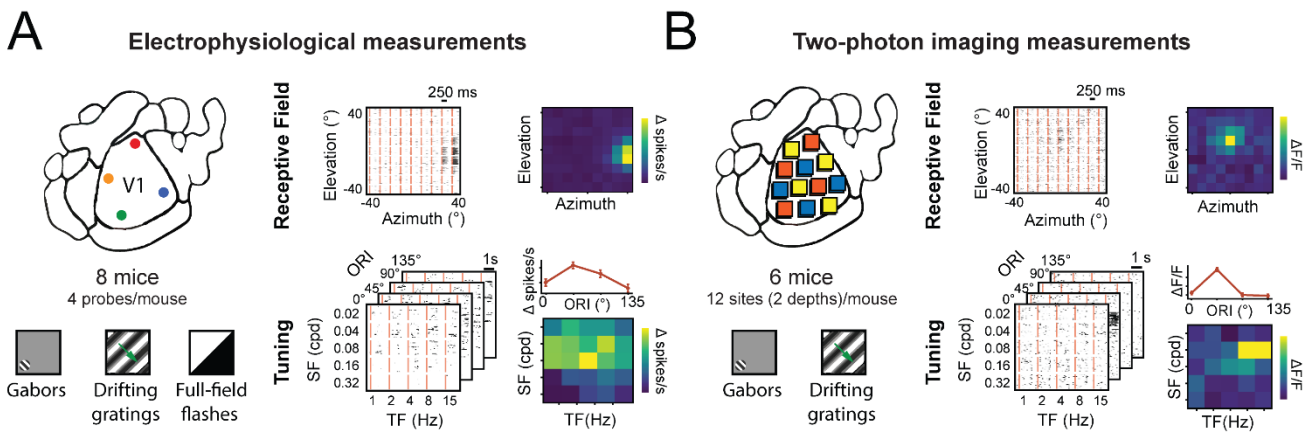

Figure 4: A new OpenScope dataset provides a within-area benchmark for functional variation across mouse visual cortex. This enables testing aspects of the unified V2 hypothesis. **A)** Electrophysiological recordings sampled four locations within V1 using Neuropixels probes, in each of eight mice. Visual stimuli included localized Gabors for spatial receptive-field mapping, full-field drifting gratings for characterization of orientation (ORI), spatial-frequency (SF), and temporal-frequency (TF) tuning, and full-field flashes. Example stimulus grids and response maps illustrate the spatial receptive-field and feature-tuning measurements obtained from the recordings. **B)** Two-photon calcium imaging sampled 12 locations distributed across V1 in each of six mice, with each location imaged at two cortical depths. Visual stimuli included localized Gabors for spatial receptive-field mapping and full-field drifting gratings for characterization of orientation, spatial-frequency, and temporal-frequency tuning.

As an initial application of this resource, we used the OpenScope electrophysiology dataset to ask whether hierarchy-associated functional differences among conventionally defined HVAs exceed the variation observed within V1, an established single cortical area (Figure 5). Under the unified-V2 hypothesis, these HVAs would represent different regions of a single V2 occupying a common hierarchical level above V1. If, instead,

bioRxiv preprint doi: https://doi.org/10.1101/2024.10.10.617533; this version posted October 1, 2026. The copyright holder for this preprint (which was not certified by peer review) is the author/funder, who has granted bioRxiv a license to display the preprint in perpetuity. It is made available under a CC-BY 4.0 International license.

conventional HVAs correspond to distinct positions along the visual cortical hierarchy, we would expect variation among HVAs in hierarchy-associated response properties to exceed the regional heterogeneity found within V1. This analysis therefore provides a quantitative within-area benchmark for interpreting functional differences among HVAs, rather than a standalone criterion for defining areal boundaries.

We examined three response properties previously associated with visual cortical hierarchy: response latency (time to first spike, TTFS), phase modulation (log10 F1/F0), and response decay timescale (Siegle et al., 2021). We quantified them using implementations adapted to improve comparability between datasets (Methods). For the within-V1 benchmark, OpenScope recordings were grouped into anterior, lateral, posterior, and medial locations (Figure 5B). For the across-HVA comparison, we analyzed recordings from LM, RL, AL, PM, and AM in the Allen Brain Observatory Visual Coding–Neuropixels dataset used by Siegle et al. (2021) (Figure 5A). Hereafter, “region” refers either to one of the four sampled V1 locations or to one of the five conventionally named HVAs.

We first tested whether these measures could detect the expected broad distinction between V1 and higher visual cortex. Using Visual Coding dataset sessions containing simultaneous recordings from V1 and HVAs, the pooled HVA population had longer TTFS than V1 by 5.45 ms (95% bootstrap interval, 3.07–7.85 ms), longer response timescales by 4.77 ms (2.31–7.37 ms), and weaker phase modulation (Δlog10 F1/F0 = −0.0898; −0.1087 to −0.0705) (Figure 5E, left). Thus, all three measures distinguished V1 from higher visual cortex under matched recording conditions. This positive control confirms that the selected metrics capture the broad functional separation expected between V1 and the next level of visual cortical processing, regardless of whether higher visual cortex is treated as one area or several.

Having established this sensitivity, we next asked whether the differences among individual HVAs were larger than regional differences within V1. For each response measure, we estimated session-adjusted means for each region and quantified the spread among these means using their standard deviation (SD). We then directly compared across-HVA and within-V1 heterogeneity by subtracting the within-V1 SD from the across-HVA SD; positive values therefore indicate greater variation across HVAs. The across-HVA-minus-within-V1 differences were 1.45 ms for TTFS (95% bootstrap interval, −0.30 to 2.13 ms), −0.0124 for phase modulation (−0.0257 to 0.0031 log10 F1/F0 units), and 1.32 ms for response timescale (−1.01 to 2.93 ms) (Figure 5E, right). All three intervals included zero. Thus, at the level of regional mean responses, differences among HVAs were not clearly greater than differences among sampled locations within V1.

We then asked the same question at the level of individual neurons. Regional means alone do not indicate how strongly populations are segregated: even relatively large differences among means may account for little of the total variation when neuronal responses within each region are broadly distributed. Indeed, single-neuron distributions were broad and strongly overlapping across both V1 locations and HVAs (Figure 5C–D). We therefore quantified the fraction of neuronal variance associated with region identity using bias-corrected omega-squared (ω^2; Methods). Within V1, recording location did not explain a significant fraction of variation in TTFS, phase modulation, or response timescale (Bonferroni-adjusted p = 1.000, 0.306, and 1.000, respectively). Across HVAs, HVA identity explained significant variation in TTFS and response timescale, but not phase modulation (adjusted p = 0.0024, 0.0012, and 0.678, respectively).

However, significance within one population and nonsignificance within another do not establish that the two effect sizes differ. The relevant test is therefore the direct comparison between them. The inter-HVA-minus-intra-V1 differences in ω^2 were 1.82 percentage points for TTFS (95% bootstrap interval, −0.74 to 3.44), −0.65 for phase modulation (−2.00 to 0.21), and 1.68 for response timescale (−0.62 to 3.39). All three intervals included zero (Figure 5F). Thus, although HVA identity accounted for detectable neuronal variation in two of the three measures, its contribution was not clearly greater than that associated with sampling different locations within V1.

bioRxiv preprint doi: https://doi.org/10.1101/2024.10.10.617533; this version posted October 1, 2026. The copyright holder for this preprint (which was not certified by peer review) is the author/funder, who has granted bioRxiv a license to display the preprint in perpetuity. It is made available under a CC-BY 4.0 International license.

Together, the three analyses provide a consistent picture. The selected response properties clearly distinguish V1 from higher visual cortex as broad groups, demonstrating sensitivity to the major hierarchical transition between them. Within higher visual cortex, however, neither the spread of regional means nor the fraction of single-neuron variance associated with region was significantly greater across HVAs than across locations within V1. These results do not imply that HVAs are functionally identical, nor do they establish that higher visual cortex is a single area. Rather, for the three hierarchy-associated properties examined here, the magnitude of functional differentiation among HVAs does not clearly exceed the heterogeneity observed within an established single cortical area. The results are therefore compatible with the possibility that conventionally defined HVAs represent functionally heterogeneous subdivisions of a complex V2.

This conclusion complements the retinotopic analysis above. Figure 3 showed that many reported functional differences across higher visual cortex are structured by visual-field position; the present analysis shows that, for three additional hierarchy-associated properties, regional differentiation does not clearly exceed the within-area benchmark provided by V1. Neither result excludes additional, retinotopy-independent specialization among HVAs. Anatomical and connectional differences could provide such independent evidence, and we consider those next.

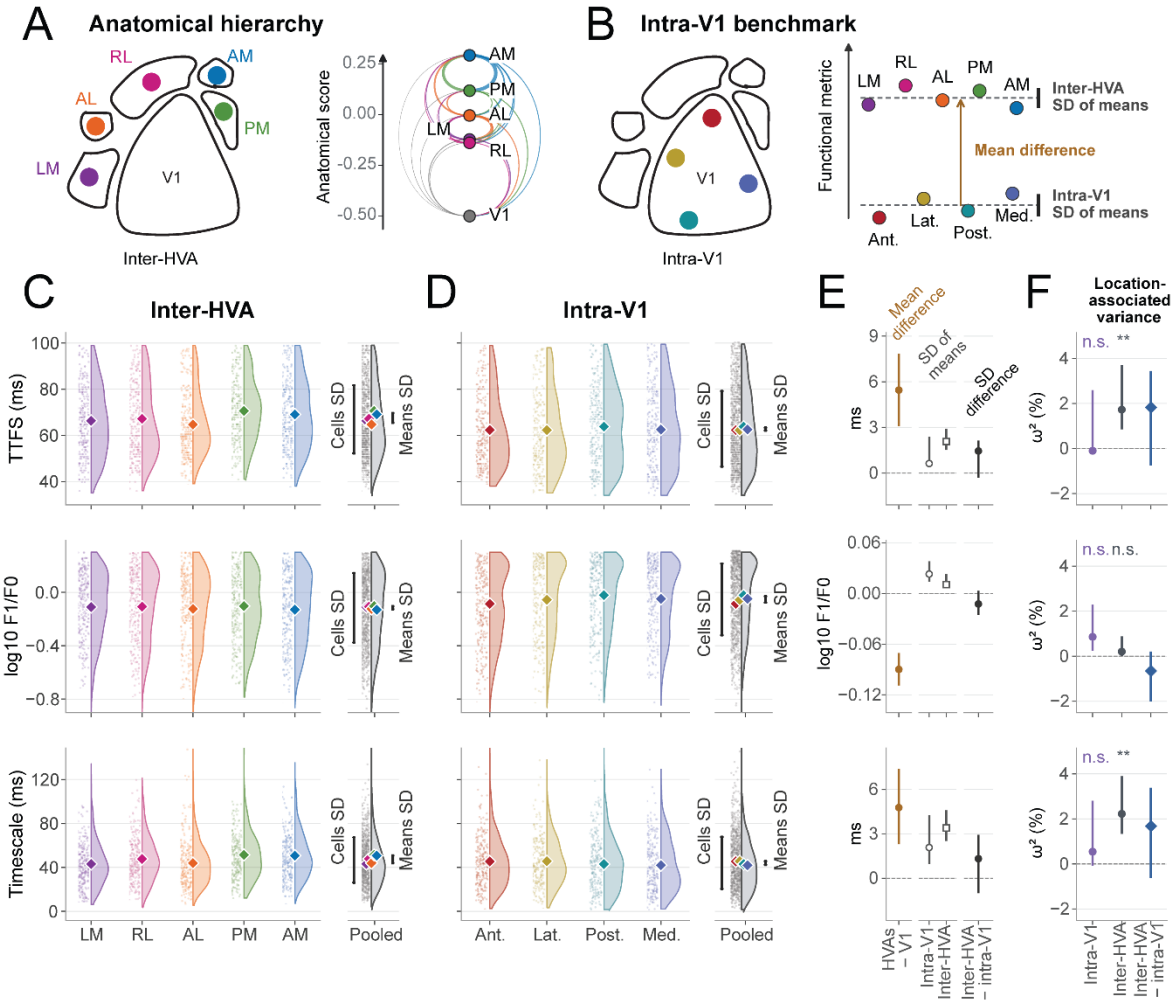

bioRxiv preprint doi: https://doi.org/10.1101/2024.10.10.617533; this version posted October 1, 2026. The copyright holder for this preprint (which was not certified by peer review) is the author/funder, who has granted bioRxiv a license to display the preprint in perpetuity. It is made available under a CC-BY 4.0 International license.

Figure 5: Large-scale OpenScope recordings provide a within-area benchmark for functional heterogeneity. **A)** Anatomical-hierarchy schematic (right) adapted from Harris et al. (2019) showing the published scores for V1 and 5 HVAs studied by Siegle et al. (2021). **B)** The four spatially separated V1 sampling regions in the new OpenScope electrophysiology dataset give us a within-area benchmark for variation among HVA means (right). Cortical outlines, sampling markers and the schematic responses are illustrative. **C–D)** Single-neuron time to first spike (TTFS), phase modulation (log10 F1/F0), and neuronal response decay timescale across **(C)** the five higher visual areas (LM, RL, AL, PM, and AM) in the Allen Brain Observatory Visual Coding–Neuropixels dataset and **(D)** four V1 sampling locations in the OpenScope electrophysiology dataset. Dots show subsamples of eligible neurons and half-violins show their distributions. Colored diamonds indicate session-adjusted group means, weighted to balance contributions across categories, animals and recordings. Within each population, means were recentered for display without changing their differences or SD (Methods). Pooled plots (grey, right) show distributions of individual-neuron values and fitted regional means. Bars span ±1 SD around the pooled-cell mean ("Cells SD") and the average regional mean ("Means SD"). **E)** Point estimates with 95% confidence intervals from 5000 whole-animal bootstrapped resamples. Left: pooled-HVA-minus-V1 mean differences from simultaneous Visual Coding recordings, serving as a positive control. Middle: SDs of regional means within V1 (OpenScope; open circles) and across HVAs (Visual Coding; open squares). Right: inter-HVA standard deviation minus intra-V1 standard deviation. For timescale, D shows one OpenScope subsampling draw; OpenScope-based estimates in E–F incorporate all ten draws (Methods). **F)** Location-associated variance estimated using bias-corrected omega-squared (ω^2): intra-V1 (purple circles), inter-HVA (dark-gray circles), and inter-HVA minus intra-V1 (blue diamonds). Component estimates are percentages of total neuronal variance; differences are expressed in percentage points. Whiskers show pointwise 95% whole-animal bootstrap intervals. Component significance labels derive from one-sided within-session block-label permutation tests, Bonferroni-adjusted across six comparisons: **, adjusted $p < .01$; n.s., adjusted $p \geq .05$. Across-HVA-minus-within-V1 differences are evaluated using bootstrap intervals.

Anatomical and connectional distinctions may reflect both areal boundaries and within-area organization

Efforts to understand the organization of the mouse visual system were largely based on prior anatomical and functional measurements in primates. Early parcellations of the mouse visual cortex were made based on cytoarchitectural features including cell density and laminar distribution, in addition to electrophysiological measurements of retinotopy - leading to the delineation of two subcomponents of a single area V2 (Glickfeld & Olsen, 2017). Subsequent work identified structural differences within higher visual cortex, including a particularly clear transition in m2AChR expression and cytoarchitecture at the border between LM and AL (Wang et al., 2011). This transition coincides with a retinotopic reversal mapped using receptive fields in the lower visual field and represents some of the strongest convergent evidence for a conventional HVA boundary, albeit one that is not obviously repeated across the broader HVA parcellation. At the same time, molecular and cytoarchitectonic heterogeneity can also occur within established visual areas. For example, m2AChR expression is nonuniform within V1 and other visual regions and is associated with functionally distinct circuits (Ji et al., 2015; Meier et al., 2025). Thus, structural differences are informative for areal delineation, but their significance is strongest when they form reproducible boundaries that coincide with independent transitions in topography, connectivity, or function.

Later parcellations of mouse visual cortex integrated cytoarchitecture with the topographic organization of anterograde projections from V1 and callosal connections. These studies provided important evidence for reproducible subdivisions within higher visual cortex. However, spatially segregated projection zones are not uniquely diagnostic of separate cortical areas: as illustrated by our model (Figure 2) and by complex retinotopic maps in other species (see Figure 6), a single continuous area can generate multiple projection patches when retinotopy is nonlinear. Thus, projection modularity provides evidence for cortical organization, but its interpretation as an areal boundary depends on its relationship to topography and other independent features. Callosal organization provides an additional spatial anchor for these maps. Wang and Burkhalter (2007) showed that LM and AL lie within a callosal-free region surrounded by callosal connections associated with vertical-meridian representations. Such organization constrains the underlying retinotopic map, although it does not by itself distinguish the LM–AL boundary.

bioRxiv preprint doi: https://doi.org/10.1101/2024.10.10.617533; this version posted October 1, 2026. The copyright holder for this preprint (which was not certified by peer review) is the author/funder, who has granted bioRxiv a license to display the preprint in perpetuity. It is made available under a CC-BY 4.0 International license.

Connectivity studies provide evidence for specialization of both kinds. Some is not reducible to retinotopic sampling: Glickfeld et al. (2013) found that V1 axons targeting different HVAs exhibit distinct visual response properties matched to their target, which could not be explained by organization within V1. This provides strong evidence that V1 inputs to different HVAs are functionally selected, although the contribution of retinotopic sampling within V1 cannot be fully separated without receptive-field measurements of the projecting boutons. Other connectional differences are themselves organized by retinotopy: V1 cell-body location predicts projection target for some recipient regions (Y. Han et al., 2018), and feedback projections from most HVAs to V1 are topographically organized and spatially biased (Morimoto et al., 2021). Neither kind distinguishes areas from modules. The stripes of primate V2 likewise receive segregated input from V1 (Livingstone & Hubel, 1984, 1987), and within mouse V1 itself, interdigitated m2AChR-positive and -negative modules participate in functionally distinct cortical networks (Meier et al., 2025). Pronounced functional and connectional modules can therefore coexist within a single established visual area.

Subcortical connectivity bears on the same question, and in particular on the second source of retinotopically anchored differences outlined above. The superior colliculus and LP form a route to higher visual cortex that bypasses V1, and this route is itself retinotopically biased (Bennett et al., 2019; Calzoni et al., 2026). Bennett et al. (2019) showed that LP contains separate SC-driven and V1-driven subregions, each with its own map of visual space, and that the portion of LP connected with a given cortical area has a retinotopic bias that partly matches that area's own bias. The SC-driven subregion shares with its collicular input a preference for small moving objects and looming stimuli, prefers lower speeds and temporal frequencies than the V1-driven subregion, and is connected primarily with ventral-stream areas including LI; the V1-driven subregion prefers faster, full-field motion and is connected primarily with AL, RL, AM and PM. Calzoni et al. (2026) further showed that collicular neurons representing the upper visual field are more likely to project to LP, and that cortical inputs to upper- and lower-field regions of the colliculus are organized by visual-field position. Tohmi et al. (2014) found that differences in velocity preference among LM, AL, AM and RL survived ablation of V1 but were abolished by lesions of the SC, and that each of these areas connects with a distinct subregion of LP. Together, these findings make SC and LP plausible sources for some of the retinotopically organized differences among V2 modules, although which response properties this pathway conveys, and to which modules, is not settled: the SC-dependent property in Tohmi et al. (2014) is the high-velocity preference of anterior areas, whereas the SC-driven LP subregion in Bennett et al. (2019) prefers low speeds and is connected mainly with lateral areas. Consistent with continuous rather than area-specific organization, Juavinett et al. (2020) found that LP inputs to retinotopically matched cortical locations vary gradually around the V1 border. Thus, where connectivity differences among HVAs are themselves retinotopically organized, they may be a source of the functional gradients rather than evidence of areal boundaries.

Another anatomical feature used to delineate the primate visual cortical hierarchy is the asymmetry between feedforward and feedback projections, which in primates terminate preferentially in Layer 4 (L4) or outside L4, respectively. In mice the laminar distinction is weaker, but D'Souza et al. (2022) identified a mouse-specific pattern: feedforward projections from V1 terminate in a column with sparse input to L1, whereas feedback projections to V1 are bistratified, preferentially targeting L1, 5 and 6 with weaker input to L2-4. They quantified this with an optical density ratio (ODR) of axon labeling in L2-4 relative to L1+(L2-4). By this measure, feedforward projections from V1 (ODR 0.61–0.88) and feedback projections to V1 (0.14–0.48) are clearly separated, whereas connections among HVAs are frequently intermediate, and the majority of higher areas occupy equivalent hierarchical levels connected by lateral pathways. Other connectivity-based analyses likewise assign distinguishable hierarchy scores to individual HVAs, although the exact hierarchical levels and separations depend on the analysis (D'Souza et al., 2022; Harris et al., 2019). Connectivity therefore provides strong evidence for a hierarchical distinction between V1 and higher visual cortex, while the extent to which conventional HVAs constitute distinct hierarchical stages is less clear.

bioRxiv preprint doi: https://doi.org/10.1101/2024.10.10.617533; this version posted October 1, 2026. The copyright holder for this preprint (which was not certified by peer review) is the author/funder, who has granted bioRxiv a license to display the preprint in perpetuity. It is made available under a CC-BY 4.0 International license.

Functional measurements likewise do not consistently follow this anatomical ordering. Reanalyzing the Visual Coding dataset, Akella et al. (2025) found that RL departed from the hierarchy-associated trends for several measures of neuronal variability and stimulus encoding. Correlations between anatomical hierarchy scores and trial-to-trial variability or stimulus information were reported after excluding RL, which showed unusually high variability and low stimulus information.

Differences in hierarchy-associated response properties need not imply areal boundaries in any case. Our OpenScope analysis provides a within-area benchmark: for all three measures, the 95% bootstrap interval for the inter-HVA-minus-intra-V1 difference in ω^2 included zero, providing no clear evidence that HVA identity explained a larger fraction of neuronal variance than recording location within V1. This does not mean that such differences are absent, or that the target-specific and subcortical pathways described above do not generate real differences in response properties; it means that, for the three measures tested, variation across HVAs did not significantly exceed that observed across sampled locations within V1. The relevant question is therefore not whether anatomical and connectional differences exist among HVAs, but whether they form reproducible, coincident discontinuities sufficient to define independent cortical areas.

Complex retinotopy beyond V1 is a common feature of secondary visual cortex in multiple species

The visual cortex immediately adjacent to V1 of several species contains modular organization with multiple reversals – as in the mouse visual cortex. These include tree shrews as previously mentioned, but also ferrets (Manger et al., 2002), and macaques (Roe & Ts'o, 1995): adjacent functional stripes in macaque V2 have been reported to represent visual-field regions with significant overlap (Roe & Ts'o, 1995). When considering the visible portions of V1 and V1-bordering visual cortex, these species share a broad organizational feature: relatively simple retinotopy in V1 is followed by more complex and modular retinotopy beyond V1 (Figure 6). However, despite the presence of multiple visual-field reversals as in the mouse, the current classification of visual cortex (Figure 6, blue box) includes a single area V2 in the tree shrew, squirrel, and macaque visual cortex. In the ferret visual cortex, the portion shown in Figure 6 contains areas 18 and 19 (Manger et al., 2002). This is in contrast to the current classification of the mouse visual cortex, which includes many more areas bordering V1. Many of these areal boundaries are based on visual field reversals (Figure 6A), though several areas have boundaries defined by convergent architectonic and functional differences. These cross-species comparisons do not establish that mouse higher visual cortex must share the same organization. Rather, they demonstrate that internal reversals are compatible with single cortical areas and therefore cannot determine areal boundaries without convergent evidence from additional factors. The examples below illustrate how retinotopy is considered alongside architectonics, connectivity, and function when defining secondary visual areas in other species.

bioRxiv preprint doi: https://doi.org/10.1101/2024.10.10.617533; this version posted October 1, 2026. The copyright holder for this preprint (which was not certified by peer review) is the author/funder, who has granted bioRxiv a license to display the preprint in perpetuity. It is made available under a CC-BY 4.0 International license.

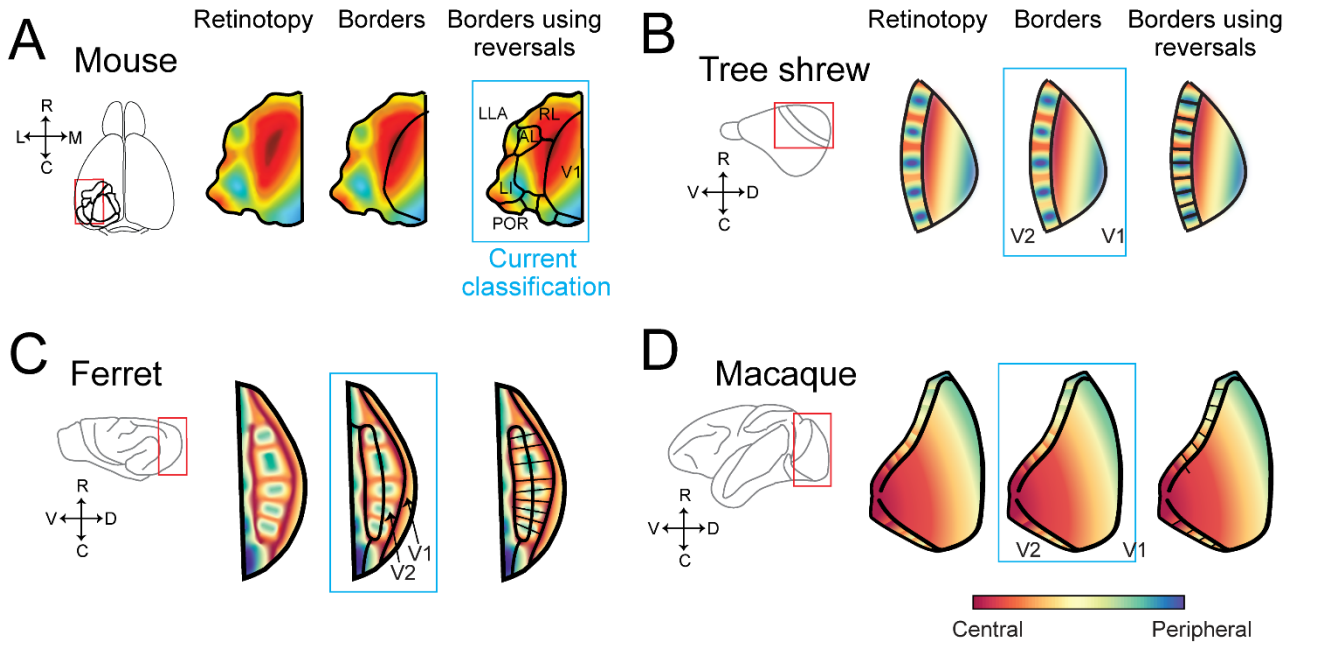

Figure 6: Complex retinotopy beyond V1 is a common feature of secondary visual cortex in multiple species. A) Retinotopy maps in mouse visual cortex, schematics created based on data from (Zhuang et al., 2017)**.** Hypothetical borders using reversals alone are shown on the right. These borders are similar to the currently accepted area delineations shown in the blue box. **B)** Retinotopic maps in tree shrew visual cortex. Data from (Sedigh-Sarvestani et al., 2021). **C)** Retinotopic maps in ferret visual cortex. Data from (Manger et al., 2002). **D)** Schematic of retinotopic maps in the visible portion of macaque V1 and V2. Data from (Roe & Ts'o, 1995; Shipp & Zeki, 2002b). Color maps are different for each species and are simply meant to indicate relatively more central or peripheral regions of the visual field.

In tree shrews (Figure 6B), the visual cortex adjacent to V1 exhibits a modular organization, with retinotopic stripes that alternate between representations of relatively more central and relatively more peripheral regions of the visual field. In the middle of each stripe lies a visual field reversal. However, a unified V2 is defined in the tree shrew which subsumes these reversals. The rationale for this delineation includes cytoarchitecture, projections from V1, and cross-hemispheric projections (Kaas et al., 1972; Sesma et al., 1984; Wong & Kaas, 2009). In addition, despite the modular appearance of the retinotopy map, the visual field is represented in V2 by a single continuous transformation, with azimuth following a sinusoidal progression and elevation a smooth one, such that the alternating bands are folds of one map rather than separate maps (Sedigh-Sarvestani et al., 2021). Thus, tree shrew V2 provides a clear example in which a modular map containing multiple reversals nonetheless forms a single continuous visual field representation within one anatomically defined area. Furthermore, functional property differences observed in V2 stripes are also related to their different retinotopic biases (Sedigh-Sarvestani et al., 2021).

In ferrets (Figure 6C), a similar modular representation was observed beyond V1, with repeated modules of crossings between more central and peripheral regions of the visual field. Within each central or peripheral module lies a visual field reversal. Thus, in ferret visual cortex, internal retinotopic reversals are distinguished from an areal boundary using convergent evidence from topography, architecture, connectivity, and function (Dell et al., 2019; Innocenti et al., 2002; Manger et al., 2002). As in tree shrews, each area contains complex internal retinotopy, with individual modules representing restricted portions of visual space (Manger et al., 2002). Similar complexity is present in the visual cortex of other carnivores. In the cat, areas 18 and 19 contain systematic but nonlinear transformations of visual space, including complex map geometry (Mallot, 1985; Tusa et al., 1979). Modeling work proposed that such complex retinotopy can arise during development as a consequence of the shape of the extrastriate cortical sheet, and that multiple stable solutions could account for inter-individual

bioRxiv preprint doi: https://doi.org/10.1101/2024.10.10.617533; this version posted October 1, 2026. The copyright holder for this preprint (which was not certified by peer review) is the author/funder, who has granted bioRxiv a license to display the preprint in perpetuity. It is made available under a CC-BY 4.0 International license.

variability in the cat, as well as other species (Wolf et al., 1994). Thus, across carnivores, complex retinotopic features can exist within individual visual areas.

A series of elegant papers in the 1980s and 1990s showed a modular, striped, organization in macaque V2 (Hubel & Livingstone, 1987; Roe & Ts'o, 1995; Shipp & Zeki, 2002a). The stripes exhibited distinct functional feature preferences, including for color, motion, and horizontal disparity. The underlying retinotopic map has been less clearly defined, in part due to the lack of optical imaging measurements in macaque V2. Published reports based on electrode penetrations across V2 indicate multiple reversals between relatively more foveal or peripheral regions of the visual field (Roe & Ts'o, 1995; Shipp & Zeki, 2002b). Regardless of the precise geometry of these internal retinotopic transformations, macaque V2 provides a clear example in which pronounced functional modularity—encompassing differences in color, motion, and disparity processing—exists within a single established cortical area. These functional subdivisions are therefore treated as modules of V2 rather than independent cortical areas.

Comparisons within rodents are particularly informative because the organization proposed for mouse visual cortex is not universal across the order. In the Eastern gray squirrel, electrophysiological mapping identified a single V2 (area 18) bordering V1, with a systematic representation of the contralateral visual hemifield that approximately mirrors V1 (Hall et al., 1971). Subsequent anatomical and connectional studies supported this organization while also revealing substantial modular structure within V2 (Gould, 1984; Kaas et al., 1989). A broadly similar V2 organization has been described in the California ground squirrel (Negwer et al., 2017). Outside the squirrel lineage, the visually specialized agouti likewise has an architectonically and physiologically defined V2 bordering V1, with an orderly representation of the contralateral visual field (Elston et al., 2006; Picanço-Diniz et al., 1989). Squirrels are often considered a relatively conservative rodent group, closer to the ancestral condition (Rosa & Krubitzer, 1999) and both squirrels and agoutis are more visually specialized than mice. It would therefore be surprising if the nocturnal mouse, with its smaller visual cortex, had independently evolved a more elaborate parcellation of extrastriate cortex than these diurnal, highly visual relatives (Laramée & Boire, 2014; Rosa & Krubitzer, 1999). An alternative is that mouse extrastriate cortex shares the V2-centered organization seen in other rodents, and that some of its proposed areas are modules within it.

The comparisons above do not imply that secondary visual cortex must follow an identical blueprint across mammals; species-specific factors such as evolutionary lineage, visual field geometry, cortical sheet geometry and binocular overlap may influence map organization. The complex V2 map of the lateral-eyed tree shrew and squirrel, however, suggests that strong binocularity is not a prerequisite for internal retinotopic reversals. In summary, complex and modular retinotopy beyond V1 occurs in several evolutionarily distant mammals, but the resulting modules are not uniformly treated as independent areas. These comparisons demonstrate that field-sign reversals, redundant representations, and functional modularity must be interpreted in the context of other anatomical, connectional, and functional evidence. They therefore motivate reconsideration of the criteria applied to mouse higher visual cortex.

Discussion:

Here we reassess the organization of mouse higher visual cortex using computational modeling, synthesis and re-analysis of published anatomical and functional evidence, and new large-scale measurements across V1. Comparative anatomical and retinotopic evidence provides an important empirical precedent for our proposal: visual-field reversals can occur within a region defined as a single visual area by independent anatomical criteria, as demonstrated most clearly in tree shrew V2 (Figure 1). Our simulations show that an explicitly defined single visual area can similarly generate internal reversals, redundant representations, and spatially segregated projection zones when constrained by the anatomical geometry of the mouse visual cortex (Figure 2). Thus,

bioRxiv preprint doi: https://doi.org/10.1101/2024.10.10.617533; this version posted October 1, 2026. The copyright holder for this preprint (which was not certified by peer review) is the author/funder, who has granted bioRxiv a license to display the preprint in perpetuity. It is made available under a CC-BY 4.0 International license.

features commonly used to identify mouse HVAs are geometrically compatible with a single complex map. We further show that several functional differences among conventionally defined HVAs covary with their systematic biases in visual-field representation (Figure 3), while analysis of our new OpenScope dataset (Figure 4) shows that variation among HVAs in several hierarchy-associated response properties does not significantly exceed variation across locations within V1 (Figure 5). Finally, our cross-species comparison shows that complex, modular retinotopy beyond V1 is common across mammals and that internal reversals are often incorporated within single cortical areas when anatomical, connectional, and functional evidence supports continuity (Figure 6). Together, these observations motivate considering a model in which many conventional mouse HVAs are spatially organized, functionally distinct subdivisions of a larger area V2.

The possibility that some proposed higher visual areas in the mouse extrastriate cortex may instead be subdivisions of a larger secondary visual area is not new. In rats, Malach (1989) proposed that the multiple V1 projection zones lateral to V1 are likely modules of a single area V2, and a similar interpretation had been made by Kaas et al. (1989) in squirrels, relevant as diurnal and highly visual rodents. The theoretical work of Wolf et al. (1994) offered a possible mechanism for such complex retinotopic organization: a single elongated visual area could develop a complex retinotopic map with multiple modules rather than one smooth map. Rosa and Krubitzer (1999) later framed the question as a choice between a "simple" hypothesis, in which V1 is bordered laterally by a single V2, and a "complex" hypothesis, in which V1 is bordered by multiple areas. They argued that comparative evidence clearly favors the simple hypothesis. Krubitzer and Huffman (2000) suggested that cortical modules may represent intermediate stages in the emergence of new cortical areas, an idea later reviewed in the context of mouse and squirrel visual cortex (Laramée & Boire, 2014). Striedter and Northcutt (2020) noted that the unusual spatial arrangement of the numerous proposed mouse visual areas, relative to primates, leaves open the possibility that some are modules rather than independent areas. Kaas et al. (2021) likewise highlighted an alternative interpretation in which the cortex bordering V1 in rats and mice comprises just two areas, V2 and a medially located prostriata. Our proposal therefore revisits a longstanding alternative rather than introducing the unified-V2 idea de novo. What we add is a synthesis of these ideas with evidence that was not previously available: modern retinotopic mapping and quantitative modeling across additional species, together with large-scale functional datasets from mouse visual cortex.

At the center of this debate is the question of what evidence is sufficient to define a cortical area (Petersen et al., 2024; Rosa, 2002). Retinotopy has been exceptionally useful for parcellating visual cortex, but comparative data demonstrate that field-sign reversals and some retinotopic redundancy can occur within established single areas. Conversely, molecular, functional, and connectional heterogeneity can also occur within individual areas. We therefore suggest that none of these observations should be considered in isolation. Instead, evidence for an areal boundary is strongest when independent features, including topography, architectonics, connectivity, and function, show reproducible and spatially coincident transitions. While the boundaries of several conventionally defined HVAs in the mouse, such as areas LM and AL, are clearly defined by factors beyond retinotopy, the delineation of several other areal boundaries currently relies heavily on retinotopy and related connectivity. Cortical area definitions are necessarily operational: they are useful conventions developed by the field to describe biological organization, and those conventions should evolve as new measurements reveal forms of organization that were not anticipated when earlier criteria were formulated. Our goal is therefore not to replace one rigid definition with another, but to make the criteria explicit and stimulate discussion about how they should be applied consistently across datasets and species.

The OpenScope dataset released with this study is intended to facilitate this broader discussion (Figure 4). Here we present only an initial analysis of this resource. By releasing the complete dataset and analysis tools, we hope to enable independent tests of the hypotheses proposed here, including analyses that challenge our interpretation. In particular, these data provide a within-area benchmark for asking how much functional

bioRxiv preprint doi: https://doi.org/10.1101/2024.10.10.617533; this version posted October 1, 2026. The copyright holder for this preprint (which was not certified by peer review) is the author/funder, who has granted bioRxiv a license to display the preprint in perpetuity. It is made available under a CC-BY 4.0 International license.

heterogeneity can occur without implying an areal boundary. More broadly, this type of quantitative comparison provides one way to distinguish between the competing models of mouse higher visual cortex.

The unified-V2 and multi-area models make several experimentally distinguishable predictions. Evidence for distinct HVAs would be strengthened by reproducible boundaries at which multiple independent properties change together: retinotopy-controlled functional discontinuities, coincident cytoarchitectonic or molecular transitions (Wang et al., 2011), abrupt changes in connectivity across conventional borders at matched receptive-field locations, or hierarchical discontinuities aligned with those borders. Demonstrating complete and independently organized visual-field maps within individual HVAs, without the orderly inter-area biases predicted by a continuous map, would provide additional support for the multi-area interpretation. Conversely, the unified-V2 hypothesis would be favored if cellular-resolution mapping reveals a continuous, albeit complex, retinotopic transformation across conventional HVA boundaries; if functional and connectional properties vary continuously across those boundaries (Figure 3) or are better predicted by retinotopic position than by HVA identity; and if the magnitude of differences among subdivisions is comparable to heterogeneity found within an established single area such as V1. Our initial analysis of the OpenScope dataset collected from several positions in V1 provides one example of this comparison: across three hierarchy-associated response properties, variation among HVAs did not significantly exceed the variance found within V1 (Figure 5).

A separate question is where the retinotopically organized differences in higher order visual cortex come from. As outlined above, they could be inherited from retinotopically anchored functional response properties in V1 or SC/LP or generated within higher visual cortex itself. Identifying these sources would not, by itself, determine whether conventionally defined HVAs belong to one area or several. Understanding the source(s) would, however, tell us how the functional organization of higher visual cortex is built, whichever model is correct. Distinguishing among the sources requires functional properties measured as a function of retinotopic position within V1 and within SC and LP, under stimulus conditions matched to recordings in higher visual cortex. The OpenScope dataset released here provides the V1 half; the existing SC and LP literature, which does not agree on which properties the pathway conveys or to which regions, does not yet provide the other. If V1 proves not to contain the gradients seen across higher visual cortex, that would argue against their simple inheritance from V1 while leaving the unified-V2 hypothesis intact.

We believe in the value and urgent need for cross-species comparisons in neuroscience. More than the particular nomenclature ultimately adopted, we think the important issue is that the assumptions underlying cortical parcellation are made explicit and continually tested against new data. Complex retinotopy in tree shrews, primates, ferrets, and other mammals has already required revisions to our conception of retinotopy. Mouse visual cortex now provides an opportunity to ask how retinotopy, function, architecture, and connectivity should be integrated into a common framework for defining cortical areas. We view the unified-V2 hypothesis as one testable proposal within that broader effort. By making both the hypothesis and the underlying OpenScope dataset available, we hope to encourage a community discussion that ultimately leads to more quantitative, reproducible, and biologically meaningful criteria for cortical area delineation across species.

Materials and Methods:

Model geometry and visual field extent (Figure 2). The modeled visual-field domain was represented by a smooth synthetic envelope constrained by electrophysiological measurements of mouse V1 from Wagor et al. (1980; approximately 0–140° azimuth and −40–60° elevation) and by the rounded shape of visual-field coverage reported by Garrett et al. (2014). The modeled cortical footprint surrounding V1 was derived from the population retinotopic maps of Waters et al. (2019). For each animal, we measured the contiguous extrastriate extent along outward normals from the V1 border. Measurements from repeated sessions were first averaged within mouse,

bioRxiv preprint doi: https://doi.org/10.1101/2024.10.10.617533; this version posted October 1, 2026. The copyright holder for this preprint (which was not certified by peer review) is the author/funder, who has granted bioRxiv a license to display the preprint in perpetuity. It is made available under a CC-BY 4.0 International license.

and the median extent across mice was then projected along corresponding normals from a common V1 contour to generate the outer cortical boundary used in the simulations.

Retinotopic registration and spatial- and temporal-frequency analysis (Figure 3F–G). We reanalyzed the Han et al. (2022) dataset using the reliable-cell flags and fitted tuning parameters supplied with the data. Two-photon cell coordinates were aligned to each animal's widefield map and then to a common cortical map. Digitized azimuth and elevation maps from Zhuang et al. (2017) were aligned to this common map using an affine transformation, and each cell was assigned the azimuth and elevation at its registered cortical location. These values therefore represent registration-based estimates of retinotopic position rather than independently measured single-cell receptive-field centers. Azimuth was limited to 0–100° and elevation to −40–40°. Eccentricity from the focea was calculated as $E = \sqrt{A^2 + (H - 20)^2}$, where $A$is azimuth and $H$is elevation in degrees, corresponding to a reference point at 0° azimuth and +20° elevation. Analyses included cells assigned to LM, AL, RL, AM, PM, or LI with finite tuning and retinotopic coordinates. The combined POR/P population was excluded because these areas were not separated in the source dataset. A total of 15,254 cells contributed to each plane fit.

Spatial and temporal frequencies were expressed in octaves as $z_{SF} = \log_2(SF/0.02)$and $z_{TF} = \log_2(TF/0.5)$, respectively. For each metric, we fit a plane $\mu = aE + bH + c$across individual cells. Values at or below 0.01 octaves and at or above 3.99 octaves were treated as lower- and upper-censored, respectively, relative to nominal limits of 0 and 4 octaves. Censored values were incorporated using an iterative Gaussian-tail imputation and least-squares fitting procedure in which the plane and residual scale were updated until the scale changed by less than 10^{-6}or 100 iterations were reached. All cells were equally weighted. The nominal limits correspond to 0.02–0.32 cycles/degree for SF and 0.5–8 Hz for TF; Han et al. (2022) tested TF stimuli through 16 Hz.

For the displayed tuning distributions, residuals, and mouse summaries, we included cells strictly within the corresponding analysis bounds, yielding 12,105 SF observations and 10,291 TF observations. Residuals were calculated as observed minus fitted log2 frequency ($z - \mu$), and fitted values were transformed back to physical units for display. Violin plots show kernel-density estimates of pooled cell values. Within each area, values were first averaged across cells from the same mouse; gray points show individual-mouse means, and the large white point and bar show the equally weighted mean across mice and its t-based 95% confidence interval. The numbers of contributing mice for LM, AL, RL, AM, PM, and LI were 10, 8, 8, 6, 6, and 9, respectively. Mean retinotopic-position markers were calculated from the pooled cell coordinates.

OpenScope data collection (Figure 4).

Electrophysiology

Mice received a headpost and a SHIELD cranial implant permitting repeated probe access (Bennett et al., 2024). Following recovery, animals underwent two weeks of handling and head-fixation habituation following established procedures (de Vries et al., 2020). Mice were gently handled for 1–2 min on days 1–2, followed by handling and 5–10 min of head fixation on days 3–5. On days 6–10, head-fixed visual stimulation increased progressively **from** 10 minutes to 50 minutes across 5 days. Animals were additionally habituated to the Neuropixels rig for one week, including three sessions in increasing time increments with the last habituation being comparable in length to the recording sessions. Visual cortical areas were delineated using intrinsic signal imaging (ISI) under light isoflurane anesthesia (1–1.4%). Contrast-reversing checkerboard bars swept across the visual field in four cardinal directions at 0.1 Hz. Fourier-derived azimuth and elevation maps were combined into visual-field sign maps, averaged across at least three acquisitions, and registered to cortical vascular landmarks (Garrett et al., 2014).

bioRxiv preprint doi: https://doi.org/10.1101/2024.10.10.617533; this version posted October 1, 2026. The copyright holder for this preprint (which was not certified by peer review) is the author/funder, who has granted bioRxiv a license to display the preprint in perpetuity. It is made available under a CC-BY 4.0 International license.

Recordings were performed in awake, head-fixed mice allowed to locomote on a freely rotating disc, using established multiprobe recording procedures (Durand et al., 2023). Up to six Neuropixels 1.0 probes were inserted to 3.1 mm at 200 µm/min, retracted by 100 µm to reduce tissue compression, and allowed to settle for approximately 30 min. The 384 recording sites nearest each probe tip were sampled at 30 kHz for action potentials and 2.5 kHz for local field potentials using Open Ephys. Visual stimuli were presented on a gamma-corrected, 60-Hz monitor positioned 15 cm from the right eye. Eye, face, and body videos were acquired at 60 Hz, and locomotion was monitored with a rotary encoder. Photodiode signals and digital synchronization pulses aligned stimulus presentation and behavioral measurements with neural activity. Spikes were sorted using Kilosort 4 (Pachitariu et al., 2024) and subjected to automated quality assessment. Recording locations were assigned using fluorescent probe-track reconstruction and registration to the Allen Common Coordinate Framework (Wang et al., 2020). For this, we used the IBL ephys alignment GUI (https://github.com/AllenNeuralDynamics/ibl-ephys-alignment-gui). Based on firing rate, LFP power, as well as spike cross-correlograms, we placed reference lines delineating borders of areas. Through this procedure, we consistently aligned the top of the cortex (Layers 2/3, where we expect spiking activity) using cross-correlograms. Other alignment locations such as white matter tracts, thalamus, and subcortical regions are only made when there are clear electrophysiological landmarks (i.e. a stark increase in firing rate for thalamus, a stark decrease in activity in white matter, etc). If features such as these are not present, the GUI's probe track interpolation is accepted. Notably, this interpolation is used for cortical layer assignments between Layers 2/3 and the bottom of cortex.

Two-Photon Imaging

Mice expressing GCaMP6f received a headpost and a chronic 5-mm cranial window over visual cortex using established surgical procedures (Groblewski et al., 2020). Following recovery, animals completed the handling and progressively extended head-fixation habituation described above, followed by a 30-min acclimation session on the mesoscope without visual stimulation. ISI-derived retinotopic maps were registered to live epifluorescence images using superficial vascular landmarks to identify the targeted visual areas. The objective was aligned perpendicular to the cranial window, and stage coordinates, surface images, and cellular reference images were retained to support repeated targeting of the same fields and neurons across sessions.

ISI-derived retinotopic maps were used to identify functionally defined visual areas and target locations for two-photon imaging. On the first imaging day, the ISI targeting map was registered to a high-resolution reference image of the cortical surface vasculature acquired through the cranial window. Superficial vascular landmarks, including vessel branching patterns and intersections, were used to align the ISI map with live epifluorescence images and thereby transfer the retinotopically defined target location to the cranial window. The aligned target was then localized under two-photon imaging by comparing the live 2P surface image with the registered vascular reference and ISI map. A 2P reference image of the cortical surface was acquired for each imaging site, and stage coordinates and reference images were retained to facilitate consistent targeting of the same cortical locations across subsequent imaging sessions.

Calcium imaging was performed in awake, head-fixed mice on a freely rotating disc using a dual-beam mesoscope based on the published 2P-RAM architecture (Sofroniew et al., 2016) and controlled by customized ScanImage software. Excitation was provided at 910 nm, and individual imaging fields measured 400 × 400 µm, sampled at 512 × 512 pixels and approximately 11 Hz per plane. Imaging planes sampled cortical depths spanning superficial cortex through layer V, with laser power adjusted according to depth and fluorescence intensity. Reference z-stacks extending 30 µm above and below each imaging plane, in 0.75-µm steps, supported assessment of axial stability. Imaging was synchronized with visual stimulation, locomotion, and eye and behavioral videos acquired at 30 Hz. Processing included nonrigid motion correction, correction of inter-plane fluorescence crosstalk, cellular segmentation, neuropil subtraction, and calculation of ΔF/F traces. Deconvolved

bioRxiv preprint doi: https://doi.org/10.1101/2024.10.10.617533; this version posted October 1, 2026. The copyright holder for this preprint (which was not certified by peer review) is the author/funder, who has granted bioRxiv a license to display the preprint in perpetuity. It is made available under a CC-BY 4.0 International license.

activity was estimated using OASIS (Friedrich et al., 2017). Sessions were assessed for saturation, photobleaching, motion, and synchronization failures.

Example neurons from the OpenScope datasets (Figure 4)
For the electrophysiology (Ephys) dataset example, the signal was computed as the difference in firing rate between the baseline and evoked activity, with the baseline corresponding to the grey screen epochs of the stimulus block. For the calcium imaging dataset (Ophys), the signal was the dF/F traces directly available from the repository. To display the response properties of the example neurons, the signals were aligned to the stimulus onset and averaged over the samples in the presentation window (0.25s for Ephys and 0.32s for Ophys for Gabor patches; and 1s and 1.05s for gratings, respectively), giving one response per trial. Trials sharing a stimulus condition were averaged. Receptive fields were obtained by grouping Gabor patch trials by screen position; orientation tuning by grouping grating trials by orientation (pooled across spatial and temporal frequencies), and the spatial × temporal frequency matrix was taken at the neuron's preferred orientation (orientation evoking the maximum average response).

Comparison of functional variation within V1 and across HVAs (Figure 4-5). The OpenScope electrophysiology dataset sampled four targeted locations within V1, designated anterior (probe A), lateral (E), posterior (C), and medial (B) in eight mice. The OpenScope imaging dataset sampled 12 V1 fields of view at two imaging depths in six mice; Figure 4B shows the 12 fields from a single mouse overlaid on its widefield retinotopic map.

For the functional hierarchy comparison (Figure 5), we analyzed three electrophysiological response properties previously associated with visual cortical hierarchy (Siegle et al., 2021): time to first spike (TTFS), phase modulation (log10 F1/F0), and response decay timescale. Probe locations were registered to the Allen CCFv3 atlas and only neurons anatomically assigned to V1 were included in the functional analysis, and session-by-location groups containing fewer than five eligible neurons were excluded. For comparison across higher visual areas, we also analyzed recordings from LM, RL, AL, PM, and AM in the Allen Brain Observatory Visual Coding–Neuropixels dataset described by Siegle et al. (2021). Region was treated as a categorical variable, with four sampling regions within V1 and five conventionally named HVAs. Methods were adapted from Siegle et al. (2021) to improve comparability between datasets: we used F1/F0 in place of the spectral modulation index, restricted the drifting-grating analysis to shared stimulus conditions, and subsampled OpenScope flash trials from 150 to 75 trials per polarity for the response-timescale analysis. Differences in recording conditions and neuronal sampling between datasets may nevertheless contribute to the estimated heterogeneity. The metric definitions and inclusion criteria are detailed below.

The main heterogeneity comparison used OpenScope recordings to estimate variation across locations within V1 and Visual Coding recordings to estimate variation across HVAs. V1 recordings from Visual Coding were used only in a separate positive control, which compared V1 and HVA responses recorded simultaneously under matched session conditions (Figure 5E, left).

TTFS was calculated using procedures adapted from Siegle et al. (2021) on responses to full screen flashed stimuli at each neuron’s preferred flash polarity, determined by mean spike count over 0-250ms after the recorded stimulus onset. TTFS was the median first-spike latency across the preferred-polarity trials, as measured in 1ms bins from 30 through 200ms after onset; trials without spikes in this window were omitted. Inclusion was gated on a significant (one-sided paired Wilcoxon test, Benjamini–Hochberg $q < .01$), positive response to the preferred flash polarity with mean firing rate during 30–180ms after flash onset exceeding the mean baseline rate during −100–0ms by ≥2 Hz and a TTFS < 100ms.

bioRxiv preprint doi: https://doi.org/10.1101/2024.10.10.617533; this version posted October 1, 2026. The copyright holder for this preprint (which was not certified by peer review) is the author/funder, who has granted bioRxiv a license to display the preprint in perpetuity. It is made available under a CC-BY 4.0 International license.

Phase modulation was quantified using F1/F0 (Skottun et al., 1991), rather than the spectral modulation index, to reduce sensitivity to differences in response phase across trials. Analyses used each neuron's preferred stimulus orientation and temporal frequency chosen from the restricted shared drifting-grating conditions: four orientations (0°, 45°, 90°, and 135°), five temporal frequencies (1,2,4,8,15 Hz) with spatial frequency fixed at 0.04 cycles per degree. F1/F0 was calculated as the amplitude of the first Fourier harmonic divided by the mean response over the first second of each trial, averaged across trials with nonzero mean responses, and log10-transformed.

Response decay timescale was calculated following Siegle et al. (2021) by fitting an exponential decay to the spike-count correlation curve over the interval 40-290ms after flash onset in 10ms bins. Inclusion required a timescale less than 300ms with a standard error less than 20ms and more than 50 spikes in the analysis window. OpenScope sessions were subsampled down to 75 of 150 trials per polarity, across 10 draws, to match the Visual Coding trial counts.

For each measure and population, category means (probe location in V1, or HVA area identity) were estimated using weighted linear models with additive session effects to account for session-to-session shared shifts across categories. For display in Figure 5C–D, fitted regional means were shifted by a common offset within each population to align their average with the equally weighted average of the raw regional means, preserving differences among means and their SD. Categories received equal total weight, divided equally among animals within category, recordings within animal/category, and neurons within recording/category. Spread across categories was quantified as the standard deviation of the fitted means, using denominator K, where K was four for V1 locations and five for HVAs. For timescale, the 10 draw-specific category variances were averaged before taking the square root.

To quantify the cell-level variance associated with the category identity, we used a bias-corrected one-way omega-squared (Lakens, 2013), with equal neuron weights and no session adjustments,

$$\omega^2 = \frac{SS_{\text{between}} - (K-1)MS_{\text{within}}}{SS_{\text{total}} + MS_{\text{within}}}$$

where $SS_{between}$ and SS_{total} denote the between-group and total sums of squares, respectively; MS_{within} denotes the within-group mean square, and K is the number of groups. Negative estimates were retained, and timescale ω^2 estimates were averaged across the ten draws. To test whether category explained more cell-level variation within each population than expected under shuffled labels (Figure 5F), we compared the observed omega-squared estimates to those drawn from 5000 within-session block-label permutations. Category labels were reassigned within each session, keeping all neurons from the same category together, to test the null that category labels are interchangeable within V1 and across the HVAs. The one-sided permutation p-values used a plus-one correction and were Bonferroni-adjusted across the six comparisons.

To directly compare heterogeneity across the HVAs (inter-HVAs) with that within V1 (intra-V1), we subtracted the intra-V1 estimate from the inter-HVA estimate for both SD (Figure 5E) and ω^2 (Figure 5F), with ω^2 differences expressed in percentage points. Pointwise 95% percentile confidence intervals were obtained from 5,000 whole-animal bootstrap resamples. Animals were sampled independently with replacement within each dataset, retaining the original number of animals and preserving dependence among neurons and probes within animals while estimating uncertainty associated with animal sampling. In each replicate, models were refitted and both component estimates and their differences were recalculated. For response decay timescale, one trial subsample was selected for each OpenScope session occurrence so that the draw was shared across its neurons and recording locations.

bioRxiv preprint doi: https://doi.org/10.1101/2024.10.10.617533; this version posted October 1, 2026. The copyright holder for this preprint (which was not certified by peer review) is the author/funder, who has granted bioRxiv a license to display the preprint in perpetuity. It is made available under a CC-BY 4.0 International license.

For the matched V1-HVA comparison (Figure 5E, left), the mean difference was estimated using a weighted linear model with group (V1 or pooled HVAs) membership and additive session effects. The V1 and pooled-HVA groups received equal total weight. Within each group, weight was divided equally among its constituent areas (one for V1, five for HVAs), then among animals within each area and recordings within each animal. Neurons within each area–recording combination received equal weights, but their weights could differ across recordings and areas. This balanced contributions despite unequal sampling. The analysis included 40, 28 and 50 eligible sessions for TTFS, phase modulation and response decay timescale, respectively. Sessions were not required to contain all five HVAs. Confidence intervals were estimated by resampling animals, retaining the simultaneously recorded V1 and HVA data together within each sampled animal.

Acknowledgements: We would like to thank Dr. Isaac Rhim for sharing his insights on the retinal cone opsin gradients in mouse. We thank Dr. Xu Han in the lab of Dr. Vincent Bonin for making their data and code available. We thank Marina Garrett, Mai Morimoto, and Matteo Carandini for helpful comments on an earlier version of the manuscript. We thank Fred Wolf for insightful feedback and discussion.

Data availability: The Allen Brain Observatory Visual Coding–Neuropixels dataset used for the higher visual area analyses is publicly available through the Allen Institute and was originally described by Siegle et al. (2021). The new OpenScope datasets reported here are deposited in DANDI Archive and made publicly available upon publication. Electrophysiology data are publicly available on the DANDI Archive (RRID:SCR_017571) at the following URL: https://dandiarchive.org/dandiset/001568. Two-photon imaging data are publicly available on the DANDI Archive (RRID:SCR_017571) at the following URL: https://dandiarchive.org/dandiset/001709. Analysis code will be available at [https://github.com/SarvestaniLab/OpenScope].

AI disclosure: Generative AI tools (Claude, Claude Code, ChatGPT, GitHub Copilot) were used to assist with writing and debugging analysis and visualization code, converting code from MATLAB to Python, and to improve the text of the manuscript. All AI-assisted recommendations were reviewed, tested, and validated by the authors. All analyses, results, and interpretations were performed and verified by the authors. The authors take full responsibility for the content of the manuscript.

References:

Aihara, S., Yoshida, T., Hashimoto, T., & Ohki, K. (2017). Color Representation Is Retinotopically Biased but Locally Intermingled in Mouse V1. *Frontiers in Neural Circuits*, *11*. https://doi.org/10.3389/fncir.2017.00022

Akella, S., Ledochowitsch, P., Siegle, J. H., Belski, H., Denman, D. D., Buice, M. A., Durand, S., Koch, C., Olsen, S. R., & Jia, X. (2025). Deciphering neuronal variability across states reveals dynamic sensory encoding. *Nature Communications*, *16*(1), 1768. https://doi.org/10.1038/s41467-025-56733-w

bioRxiv preprint doi: https://doi.org/10.1101/2024.10.10.617533; this version posted October 1, 2026. The copyright holder for this preprint (which was not certified by peer review) is the author/funder, who has granted bioRxiv a license to display the preprint in perpetuity. It is made available under a CC-BY 4.0 International license.

Bennett, C., Gale, S. D., Garrett, M. E., Newton, M. L., Callaway, E. M., Murphy, G. J., & Olsen, S. R. (2019). Higher-Order Thalamic Circuits Channel Parallel Streams of Visual Information in Mice. *Neuron*, *102*(2), 477-492.e5. https://doi.org/10.1016/j.neuron.2019.02.010

Bennett, C., Ouellette, B., Ramirez, T. K., Cahoon, A., Cabasco, H., Browning, Y., Lakunina, A., Lynch, G. F., McBride, E. G., Belski, H., Gillis, R., Grasso, C., Howard, R., Johnson, T., Loeffler, H., Smith, H., Sullivan, D., Williford, A., Caldejon, S., … Olsen, S. R. (2024). SHIELD: Skull-shaped hemispheric implants enabling large-scale electrophysiology datasets in the mouse brain. *Neuron*, *112*(17), 2869-2885.e8. https://doi.org/10.1016/j.neuron.2024.06.015

Calzoni, A., Sans-Dublanc, A., Kühn, N. K., Remans, D., Lopez, F. F. de C., Reinhard, K., & Farrow, K. (2026). *Visual field position shapes input sampling and output routing in the superior colliculus* (p. 2026.05.27.728073). bioRxiv. https://doi.org/10.64898/2026.05.27.728073

de Vries, S. E. J., Lecoq, J. A., Buice, M. A., Groblewski, P. A., Ocker, G. K., Oliver, M., Feng, D., Cain, N., Ledochowitsch, P., Millman, D., Roll, K., Garrett, M., Keenan, T., Kuan, L., Mihalas, S., Olsen, S., Thompson, C., Wakeman, W., Waters, J., … Koch, C. (2020). A large-scale standardized physiological survey reveals functional organization of the mouse visual cortex. *Nature Neuroscience*, *23*(1), 138–151. https://doi.org/10.1038/s41593-019-0550-9

Dell, L. A., Innocenti, G. M., Hilgetag, C. C., & Manger, P. R. (2019). Cortical and thalamic connectivity of occipital visual cortical areas 17, 18, 19, and 21 of the domestic ferret (Mustela putorius furo). *Journal of Comparative Neurology*, *527*(8), 1293–1314. https://doi.org/10.1002/cne.24631

Demb, J. B., & Singer, J. H. (2015). Functional Circuitry of the Retina. *Annual Review of Vision Science*, *1*, 263–289. https://doi.org/10.1146/annurev-vision-082114-035334

Denman, D. J., Luviano, J. A., Ollerenshaw, D. R., Cross, S., Williams, D., Buice, M. A., Olsen, S. R., & Reid, R. C. (2018). Mouse color and wavelength-specific luminance contrast sensitivity are non-uniform across visual space. *Elife*, *7*. https://doi.org/10.7554/eLife.31209

bioRxiv preprint doi: https://doi.org/10.1101/2024.10.10.617533; this version posted October 1, 2026. The copyright holder for this preprint (which was not certified by peer review) is the author/funder, who has granted bioRxiv a license to display the preprint in perpetuity. It is made available under a CC-BY 4.0 International license.

D'Souza, R. D., Wang, Q., Ji, W., Meier, A. M., Kennedy, H., Knoblauch, K., & Burkhalter, A. (2022). Hierarchical and nonhierarchical features of the mouse visual cortical network. *Nature Communications*, *13*(1), 503. https://doi.org/10.1038/s41467-022-28035-y

Durand, S., Heller, G. R., Ramirez, T. K., Luviano, J. A., Williford, A., Sullivan, D. T., Cahoon, A. J., Farrell, C., Groblewski, P. A., Bennett, C., Siegle, J. H., & Olsen, S. R. (2023). Acute head-fixed recordings in awake mice with multiple Neuropixels probes. *Nature Protocols*, *18*(2), 424–457. https://doi.org/10.1038/s41596-022-00768-6

Elston, G. N., Elston, A., Freire, M. A. M., Gomes Leal, W., Dias, I. A., Pereira, A., Silveira, L. C. L., & Picanço Diniz, C. W. (2006). Specialization of pyramidal cell structure in the visual areas V1, V2 and V3 of the South American rodent, *Dasyprocta primnolopha*. *Brain Research*, *1106*(1), 99–110. https://doi.org/10.1016/j.brainres.2006.05.100

Felleman, D. J., & Van Essen, D. C. (1991). Distributed hierarchical processing in the primate cerebral cortex. *Cerebral Cortex*, *1*(1), 1–47. https://doi.org/10.1093/cercor/1.1.1-a

Friedrich, J., Zhou, P., & Paninski, L. (2017). Fast online deconvolution of calcium imaging data. *PLOS Computational Biology*, *13*(3), e1005423. https://doi.org/10.1371/journal.pcbi.1005423

Garrett, M. E., Nauhaus, I., Marshel, J. H., & Callaway, E. M. (2014). Topography and Areal Organization of Mouse Visual Cortex. *Journal of Neuroscience*, *34*(37), 12587–12600. https://doi.org/10.1523/JNEUROSCI.1124-14.2014

Glickfeld, L. L., Andermann, M. L., Bonin, V., & Reid, R. C. (2013). Cortico-cortical projections in mouse visual cortex are functionally target specific. *Nature Neuroscience*, *16*(2), 219–226. https://doi.org/10.1038/nn.3300

Glickfeld, L. L., & Olsen, S. R. (2017). Higher-Order Areas of the Mouse Visual Cortex. *Annual Review of Vision Science*, *3*, 251–273. https://doi.org/10.1146/annurev-vision-102016-061331

Goodhill, G. J., & Willshaw, D. J. (1990). Application of the elastic net algorithm to the formation of ocular dominance stripes. *Network: Computation in Neural Systems*, *1*(1), 41–59. https://doi.org/10.1088/0954-898X_1_1_004

bioRxiv preprint doi: https://doi.org/10.1101/2024.10.10.617533; this version posted October 1, 2026. The copyright holder for this preprint (which was not certified by peer review) is the author/funder, who has granted bioRxiv a license to display the preprint in perpetuity. It is made available under a CC-BY 4.0 International license.

Gould, H. J. (1984). Interhemispheric connections of the visual cortex in the grey squirrel (Sciurus carolinensis). *Journal of Comparative Neurology*, *223*(2), 259–301. https://doi.org/10.1002/cne.902230209

Groblewski, P. A., Sullivan, D., Lecoq, J., de Vries, S. E. J., Caldejon, S., L'Heureux, Q., Keenan, T., Roll, K., Slaughterback, C., Williford, A., & Farrell, C. (2020). A standardized head-fixation system for performing large-scale, *in vivo* physiological recordings in mice. *Journal of Neuroscience Methods*, *346*, 108922. https://doi.org/10.1016/j.jneumeth.2020.108922

Groen, I. I. A., Dekker, T. M., Knapen, T., & Silson, E. H. (2022). Visuospatial coding as ubiquitous scaffolding for human cognition. *Trends in Cognitive Sciences*, *26*(1), 81–96. https://doi.org/10.1016/j.tics.2021.10.011

Hall, W. C., Kaas, J. H., Killackey, H., & Diamond, I. T. (1971). Cortical visual areas in the grey squirrel (Sciurus carolinesis): A correlation between cortical evoked potential maps and architectonic subdivisions. *Journal of Neurophysiology*, *34*(3), 437–452. https://doi.org/10.1152/jn.1971.34.3.437

Han, X., Vermaercke, B., & Bonin, V. (2022). Diversity of spatiotemporal coding reveals specialized visual processing streams in the mouse cortex. *Nature Communications*, *13*(1), 3249. https://doi.org/10.1038/s41467-022-29656-z

Han, Y., Kebschull, J. M., Campbell, R. A. A., Cowan, D., Imhof, F., Zador, A. M., & Mrsic-Flogel, T. D. (2018). The logic of single-cell projections from visual cortex. *Nature*, *556*(7699), 51–56. https://doi.org/10.1038/nature26159

Harris, J. A., Mihalas, S., Hirokawa, K. E., Whitesell, J. D., Choi, H., Bernard, A., Bohn, P., Caldejon, S., Casal, L., Cho, A., Feiner, A., Feng, D., Gaudreault, N., Gerfen, C. R., Graddis, N., Groblewski, P. A., Henry, A. M., Ho, A., Howard, R., … Zeng, H. (2019). Hierarchical organization of cortical and thalamic connectivity. *Nature*, *575*(7781), 195–202. https://doi.org/10.1038/s41586-019-1716-z

bioRxiv preprint doi: https://doi.org/10.1101/2024.10.10.617533; this version posted October 1, 2026. The copyright holder for this preprint (which was not certified by peer review) is the author/funder, who has granted bioRxiv a license to display the preprint in perpetuity. It is made available under a CC-BY 4.0 International license.

Hubel, D. H., & Livingstone, M. S. (1987). Segregation of form, color, and stereopsis in primate area 18. *Journal of Neuroscience*, *7*(11), 3378–3415. https://doi.org/10.1523/jneurosci.07-11-03378.1987

Innocenti, G. M., Manger, P. R., Masiello, I., Colin, I., & Tettoni, L. (2002). Architecture and callosal connections of visual areas 17, 18, 19 and 21 in the ferret (Mustela putorius). *Cerebral Cortex (New York, N.Y.: 1991)*, *12*(4), 411–422. https://doi.org/10.1093/cercor/12.4.411

Ji, W., Gămănuţ, R., Bista, P., D'Souza, R. D., Wang, Q., & Burkhalter, A. (2015). Modularity in the Organization of Mouse Primary Visual Cortex. *Neuron*, *87*(3), 632–643. https://doi.org/10.1016/j.neuron.2015.07.004

Juavinett, A. L., Kim, E. J., Collins, H. C., & Callaway, E. M. (2020). A systematic topographical relationship between mouse lateral posterior thalamic neurons and their visual cortical projection targets. *The Journal of Comparative Neurology*, *528*(1), 95–107. https://doi.org/10.1002/cne.24737

Kaas, J. H., Hall, W. C., Killackey, H., & Diamond, I. T. (1972). Visual cortex of the tree shrew (Tupaia glis): Architectonic subdivisions and representations of the visual field. *Brain Research*, *42*(2), 491–496. https://doi.org/10.1016/0006-8993(72)90548-3

Kaas, J. H., Krubitzer, L. A., & Johanson, K. L. (1989). Cortical connections of areas 17 (V-I) and 18 (V-II) of squirrels. *Journal of Comparative Neurology*, *281*(3), 426–446. https://doi.org/10.1002/cne.902810308

Kaas, J. H., Qi, H.-X., & Stepniewska, I. (2021). Escaping the nocturnal bottleneck, and the evolution of the dorsal and ventral streams of visual processing in primates. *Philosophical Transactions of the Royal Society B: Biological Sciences*, *377*(1844), 20210293. https://doi.org/10.1098/rstb.2021.0293

Kanwisher, N. (2001). Faces and places: Of central (and peripheral) interest. *Nature Neuroscience*, *4*(5), 455–456. https://doi.org/10.1038/87399

bioRxiv preprint doi: https://doi.org/10.1101/2024.10.10.617533; this version posted October 1, 2026. The copyright holder for this preprint (which was not certified by peer review) is the author/funder, who has granted bioRxiv a license to display the preprint in perpetuity. It is made available under a CC-BY 4.0 International license.

Krubitzer, L., & Huffman, K. J. (2000). Arealization of the neocortex in mammals: Genetic and epigenetic contributions to the phenotype. *Brain, Behavior and Evolution*, *55*(6), 322–335. https://doi.org/10.1159/000006667

La Chioma, A., Bonhoeffer, T., & Hübener, M. (2019). Area-Specific Mapping of Binocular Disparity across Mouse Visual Cortex. *Current Biology*, *29*(17), 2954-2960.e5. https://doi.org/10.1016/j.cub.2019.07.037

Lakens, D. (2013). Calculating and reporting effect sizes to facilitate cumulative science: A practical primer for t-tests and ANOVAs. *Frontiers in Psychology*, *4*. https://doi.org/10.3389/fpsyg.2013.00863

Laramée, M.-E., & Boire, D. (2014). Visual cortical areas of the mouse: Comparison of parcellation and network structure with primates. *Frontiers in Neural Circuits*, *8*, 149. https://doi.org/10.3389/fncir.2014.00149

Livingstone, M., & Hubel, D. (1984). Anatomy and physiology of a color system in the primate visual cortex. *The Journal of Neuroscience: The Official Journal of the Society for Neuroscience*, *4*(1), 309–356. https://doi.org/10.1523/JNEUROSCI.04-01-00309.1984

Livingstone, M., & Hubel, D. (1987). Connections between layer 4B of area 17 and the thick cytochrome oxidase stripes of area 18 in the squirrel monkey. *The Journal of Neuroscience*, *7*(11), 3371–3377. https://doi.org/10.1523/JNEUROSCI.07-11-03371.1987

Malach, R. (1989). Patterns of connections in rat visual cortex. *Journal of Neuroscience*, *9*(11), 3741–3752. https://doi.org/10.1523/JNEUROSCI.09-11-03741.1989

Mallot, H. A. (1985). An overall description of retinotopic mapping in the cat's visual cortex areas 17, 18, and 19. *Biological Cybernetics*, *52*(1), 45–51. https://doi.org/10.1007/BF00336934

Manger, P. R., Kiper, D., Masiello, I., Murillo, L., Tettoni, L., Hunyadi, Z., & Innocenti, G. M. (2002). The representation of the visual field in three extrastriate areas of the ferret (Mustela putorius) and the relationship of retinotopy and field boundaries to callosal connectivity. *Cerebral Cortex (New York, N.Y.: 1991)*, *12*(4), 423–437. https://doi.org/10.1093/cercor/12.4.423

bioRxiv preprint doi: https://doi.org/10.1101/2024.10.10.617533; this version posted October 1, 2026. The copyright holder for this preprint (which was not certified by peer review) is the author/funder, who has granted bioRxiv a license to display the preprint in perpetuity. It is made available under a CC-BY 4.0 International license.

Marshel, J. H., Garrett, M. E., Nauhaus, I., & Callaway, E. M. (2011). Functional specialization of seven mouse visual cortical areas. *Neuron*, *72*(6), 1040–1054. https://doi.org/10.1016/j.neuron.2011.12.004

Meier, A. M., D'Souza, R. D., Ji, W., Han, E. B., & Burkhalter, A. (2025). *Interdigitating Modules for Visual Processing During Locomotion and Rest in Mouse V1* (p. 2025.02.21.639505). bioRxiv. https://doi.org/10.1101/2025.02.21.639505

Minderer, M., Brown, K. D., & Harvey, C. D. (2019). The Spatial Structure of Neural Encoding in Mouse Posterior Cortex during Navigation. *Neuron*, *102*(1), 232-248.e11. https://doi.org/10.1016/j.neuron.2019.01.029

Morimoto, M. M., Uchishiba, E., & Saleem, A. B. (2021). Organization of feedback projections to mouse primary visual cortex. *iScience*, *24*(5), 102450. https://doi.org/10.1016/j.isci.2021.102450

Negwer, M., Liu, Y.-J., Schubert, D., & Lyon, D. C. (2017). V1 connections reveal a series of elongated higher visual areas in the California ground squirrel, Otospermophilus beecheyi. *The Journal of Comparative Neurology*, *525*(8), 1909–1921. https://doi.org/10.1002/cne.24173

Pachitariu, M., Sridhar, S., Pennington, J., & Stringer, C. (2024). Spike sorting with Kilosort4. *Nature Methods*, *21*(5), 914–921. https://doi.org/10.1038/s41592-024-02232-7

Petersen, S. E., Seitzman, B. A., Nelson, S. M., Wig, G. S., & Gordon, E. M. (2024). Principles of cortical areas and their implications for neuroimaging. *Neuron*, *112*(17), 2837–2853. https://doi.org/10.1016/j.neuron.2024.05.008

Picanço-Diniz, C. W., Oliveira, H. L., Silveira, L. C., & Oswaldo-Cruz, E. (1989). The visual cortex of the agouti (Dasyprocta aguti): Architectonic subdivisions. *Brazilian Journal of Medical and Biological Research = Revista Brasileira De Pesquisas Medicas E Biologicas*, *22*(1), 121–138.

Qiu, Y., Zhao, Z., Klindt, D., Kautzky, M., Szatko, K. P., Schaeffel, F., Rifai, K., Franke, K., Busse, L., & Euler, T. (2021). Natural environment statistics in the upper and lower visual field are reflected in mouse retinal specializations. *Current Biology*, *31*(15), 3233-3247.e6. https://doi.org/10.1016/j.cub.2021.05.017

bioRxiv preprint doi: https://doi.org/10.1101/2024.10.10.617533; this version posted October 1, 2026. The copyright holder for this preprint (which was not certified by peer review) is the author/funder, who has granted bioRxiv a license to display the preprint in perpetuity. It is made available under a CC-BY 4.0 International license.

Rhim, I., Coello-Reyes, G., Ko, H.-K., & Nauhaus, I. (2017). Maps of cone opsin input to mouse V1 and higher visual areas. *J. Neurophysiol.*, *117*(4), 1674–1682. https://doi.org/10.1152/jn.00849.2016

Rhim, I., Coello-Reyes, G., & Nauhaus, I. (2021). Variations in photoreceptor throughput to mouse visual cortex and the unique effects on tuning. *Sci. Rep.*, *11*(1), 11937. https://doi.org/10.1038/s41598-021-90650-4

Roe, A. W., & Ts'o, D. Y. (1995). Visual topography in primate V2: Multiple representation across functional stripes. *The Journal of Neuroscience: The Official Journal of the Society for Neuroscience*, *15*(5 Pt 2), 3689–3715. https://doi.org/10.1523/JNEUROSCI.15-05-03689.1995

Rosa, M. (2002). Visual maps in the adult primate cerebral cortex: Some implications for brain development and evolution. *Brazilian Journal of Medical and Biological Research*, *35*(12), 1485–1498. https://doi.org/10.1590/S0100-879X2002001200008

Rosa, M., & Krubitzer, L. A. (1999). The evolution of visual cortex: Where is V2? *Trends in Neurosciences*, *22*(6), 242–248. https://doi.org/10.1016/S0166-2236(99)01398-3

Sedigh-Sarvestani, M., & Fitzpatrick, D. (2022). What and Where: Location-Dependent Feature Sensitivity as a Canonical Organizing Principle of the Visual System. *Frontiers in Neural Circuits*, *16*, 834876. https://doi.org/10.3389/fncir.2022.834876

Sedigh-Sarvestani, M., Lee, K.-S., Jaepel, J., Satterfield, R., Shultz, N., & Fitzpatrick, D. (2021). A sinusoidal transformation of the visual field is the basis for periodic maps in area V2. *Neuron*, *109*(24), 4068-4079.e6. https://doi.org/10.1016/J.NEURON.2021.09.053

Sereno, M. I., McDonald, C. T., & Allman, J. M. (1994). Analysis of retinotopic maps in extrastriate cortex. *Cereb. Cortex*, *4*(6), 601–620. https://doi.org/10.1093/cercor/4.6.601

Sesma, M. a, Casagrande, V. a, & Kaas, J. H. (1984). Cortical connections of area 17 in tree shrews. *The Journal of Comparative Neurology*, *230*(3), 337–351. https://doi.org/10.1002/cne.902300303

Shipp, S., & Zeki, S. (2002a). The functional organization of area V2, I: specialization across stripes and layers. *Visual Neuroscience*, *19*(02), 187–210. https://doi.org/10.1017/s0952523802191164

bioRxiv preprint doi: https://doi.org/10.1101/2024.10.10.617533; this version posted October 1, 2026. The copyright holder for this preprint (which was not certified by peer review) is the author/funder, who has granted bioRxiv a license to display the preprint in perpetuity. It is made available under a CC-BY 4.0 International license.

Shipp, S., & Zeki, S. (2002b). The functional organization of area V2, II: The impact of stripes on visual topography. *Visual Neuroscience*, *19*(02), 211–231. https://doi.org/10.1017/s0952523802191176

Siegle, J. H., Jia, X., Durand, S., Gale, S., Bennett, C., Graddis, N., Heller, G., Ramirez, T. K., Choi, H., Luviano, J. A., Groblewski, P. A., Ahmed, R., Arkhipov, A., Bernard, A., Billeh, Y. N., Brown, D., Buice, M. A., Cain, N., Caldejon, S., … Koch, C. (2021). Survey of spiking in the mouse visual system reveals functional hierarchy. *Nature*, *592*(7852), 86–92. https://doi.org/10.1038/s41586-020-03171-x

Sit, K. K., & Goard, M. J. (2020). Distributed and retinotopically asymmetric processing of coherent motion in mouse visual cortex. *Nature Communications*, *11*(1), 3565. https://doi.org/10.1038/s41467-020-17283-5

Skottun, B. C., De Valois, R. L., Grosof, D. H., Movshon, J. A., Albrecht, D. G., & Bonds, A. B. (1991). Classifying simple and complex cells on the basis of response modulation. *Vision Research*, *31*(7), 1078–1086. https://doi.org/10.1016/0042-6989(91)90033-2

Sofroniew, N. J., Flickinger, D., King, J., & Svoboda, K. (2016). A large field of view two-photon mesoscope with subcellular resolution for in vivo imaging. *eLife*, *5*, e14472. https://doi.org/10.7554/eLife.14472

Striedter, G. F., & Northcutt, R. G. (2020). *Brains Through Time: A Natural History of Vertebrates*. Oxford University Press.

Tohmi, M., Meguro, R., Tsukano, H., Hishida, R., & Shibuki, K. (2014). The extrageniculate visual pathway generates distinct response properties in the higher visual areas of mice. *Current Biology: CB*, *24*(6), 587–597. https://doi.org/10.1016/j.cub.2014.01.061

Tusa, R. J., Rosenquist, A. C., & Palmer, L. A. (1979). Retinotopic organization of areas 18 and 19 in the cat. *Journal of Comparative Neurology*, *185*(4), 657–678. https://doi.org/10.1002/cne.901850405

bioRxiv preprint doi: https://doi.org/10.1101/2024.10.10.617533; this version posted October 1, 2026. The copyright holder for this preprint (which was not certified by peer review) is the author/funder, who has granted bioRxiv a license to display the preprint in perpetuity. It is made available under a CC-BY 4.0 International license.

van Beest, E. H., Mukherjee, S., Kirchberger, L., Schnabel, U. H., van der Togt, C., Teeuwen, R. R. M., Barsegyan, A., Meyer, A. F., Poort, J., Roelfsema, P. R., & Self, M. W. (2021). Mouse visual cortex contains a region of enhanced spatial resolution. *Nature Communications*, *12*(1). https://doi.org/10.1038/S41467-021-24311-5

Wagor, E., Mangini, N. J., & Pearlman, A. L. (1980). Retinotopic organization of striate and extrastriate visual cortex in the mouse. *The Journal of Comparative Neurology*, *193*(1), 187–202. https://doi.org/10.1002/cne.901930113

Wang, Q., & Burkhalter, A. (2007). Area map of mouse visual cortex. *Journal of Comparative Neurology*, *502*(3), 339–357. https://doi.org/10.1002/cne.21286

Wang, Q., Ding, S.-L., Li, Y., Royall, J., Feng, D., Lesnar, P., Graddis, N., Naeemi, M., Facer, B., Ho, A., Dolbeare, T., Blanchard, B., Dee, N., Wakeman, W., Hirokawa, K. E., Szafer, A., Sunkin, S. M., Oh, S. W., Bernard, A., … Ng, L. (2020). The Allen Mouse Brain Common Coordinate Framework: A 3D Reference Atlas. *Cell*, *181*(4), 936-953.e20. https://doi.org/10.1016/j.cell.2020.04.007

Wang, Q., Gao, E., & Burkhalter, A. (2011). Gateways of ventral and dorsal streams in mouse visual cortex. *J. Neurosci.*, *31*(5), 1905–1918. https://doi.org/10.1523/JNEUROSCI.3488-10.2011

Waters, J., Lee, E., Gaudreault, N., Griffin, F., Lecoq, J., Slaughterbeck, C., Sullivan, D., Farrell, C., Perkins, J., Reid, D., Feng, D., Graddis, N., Garrett, M., Li, Y., Long, F., Mochizuki, C., Roll, K., Zhuang, J., & Thompson, C. (2019). Biological variation in the sizes, shapes and locations of visual cortical areas in the mouse. *PLOS ONE*, *14*(5), e0213924. https://doi.org/10.1371/journal.pone.0213924

Wolf, F., Bauer, H. U., & Geisel, T. (1994). Formation of field discontinuities and islands in visual cortical maps. *Biological Cybernetics*, *70*(6), 525–531. https://doi.org/10.1007/BF00198805

Wong, P., & Kaas, J. H. (2009). Architectonic subdivisions of neocortex in the tree shrew (Tupaia belangeri). *Anatomical Record (Hoboken, N.J. : 2007)*, *292*(7), 994–1027. https://doi.org/10.1002/ar.20916

bioRxiv preprint doi: https://doi.org/10.1101/2024.10.10.617533; this version posted October 1, 2026. The copyright holder for this preprint (which was not certified by peer review) is the author/funder, who has granted bioRxiv a license to display the preprint in perpetuity. It is made available under a CC-BY 4.0 International license.

Yu, H.-H., Chaplin, T. A., & Rosa, M. (2015). Representation of central and peripheral vision in the primate cerebral cortex: Insights from studies of the marmoset brain. *Neuroscience Research*, *93*, 47–61. https://doi.org/10.1016/j.neures.2014.09.004

Yu, H.-H., & Rosa, M. (2014). Uniformity and diversity of response properties of neurons in the primary visual cortex: Selectivity for orientation, direction of motion, and stimulus size from center to far periphery. *Visual Neuroscience*, *31*(1), 85–98. https://doi.org/10.1017/S0952523813000448

Yu, H.-H., Rowley, D., Price, N., Rosa, M., & Zavitz, E. (2020). A twisted visual field map in the primate dorsomedial cortex predicted by topographic continuity. *Science Advances*, *6*(6), eaaz8763. https://doi.org/10.1126/sciadv.aaz8673

Yu, H.-H., Verma, R., Yang, Y., Tibballs, H. A., Lui, L. L., Reser, D. H., & Rosa, M. (2010). Spatial and temporal frequency tuning in striate cortex: Functional uniformity and specializations related to receptive field eccentricity. *European Journal of Neuroscience*, *31*(6), 1043–1062. https://doi.org/10.1111/j.1460-9568.2010.07118.x

Zhang, X., An, X., Liu, H., Peng, J., Cai, S., Wang, W., Lin, D.-T., & Yang, Y. (2015). The Topographical Arrangement of Cutoff Spatial Frequencies across Lower and Upper Visual Fields in Mouse V1. *Scientific Reports*, *5*(1), 7734. https://doi.org/10.1038/srep07734

Zhong, L., Baptista, S., Gattoni, R., Arnold, J., Flickinger, D., Stringer, C., & Pachitariu, M. (2025). Unsupervised pretraining in biological neural networks. *Nature*, *644*(8077), 741–748. https://doi.org/10.1038/s41586-025-09180-y

Zhuang, J., Ng, L., Williams, D., Valley, M., Li, Y., Garrett, M., & Waters, J. (2017). An extended retinotopic map of mouse cortex. *eLife*, *6*, e18372. https://doi.org/10.7554/elife.18372